UNIVERSITÀ DEGLI STUDI FIRENZE

FLORE
Repository istituzionale dell'Università degli Studi di Firenze

Acute kidney injury promotes development of papillary renal cell adenoma and carcinoma from renal progenitor cells.

Questa è la Versione finale referata (Post print/Accepted manuscript) della seguente pubblicazione:

Original Citation:

Acute kidney injury promotes development of papillary renal cell adenoma and carcinoma from renal progenitor cells / Peired AJ, Antonelli G, Angelotti ML, Allinovi M, Guzzi F, Sisti A, Semeraro R, Conte C, Mazzinghi B, Nardi S, Melica ME, De Chiara L, Lazzeri E, Lasagni L, Lottini T, Landini S, Giglio S, Mari A, Di Maida F, Antonelli A, Porpiglia F, Schiavina R, Ficarra V, Facchiano D, Gacci M, Serni S, Carini M, Netto GJ, Roperto RM, Magi A, Christiansen CF, Rotondi M, Liapis H, Anders HJ, Minervini A, Raspollini MR,

Availability:

This version is available at: 2158/1188856 since: 2020-09-03T12:06:59Z

Terms of use:

Open Access

La pubblicazione è resa disponibile sotto le norme e i termini della licenza di deposito, secondo quanto stabilito dalla Policy per l'accesso aperto dell'Università degli Studi di Firenze (https://www.sba.unifi.it/upload/policy-oa-2016-1.pdf)

Publisher copyright claim:

(Article begins on next page)

19 April 2024

Title: Acute kidney injury promotes development of papillary renal cell adenoma and carcinoma from renal progenitor cells

Authors: Anna Julie Peired[1,2], Giulia Antonelli[1,2], Maria Lucia Angelotti[1,2], Marco Allinovi[1,2,3], Francesco Guzzi[2], Alessandro Sisti[4], Roberto Semeraro[2], Carolina Conte[1,2], Benedetta Mazzinghi[4], Sara Nardi[4], Maria Elena Melica[1,2], Letizia De Chiara[4], Elena Lazzeri[1,2], Laura Lasagni[1,2], Tiziano Lottini[5], Samuela Landini[2], Sabrina Giglio[2], Andrea Mari[6], Fabrizio Di Maida[6], Alessandro Antonelli[7], Francesco Porpiglia[8], Riccardo Schiavina[9], Vincenzo Ficarra[10], Davide Facchiano[6], Mauro Gacci[6], Sergio Serni[6], Marco Carini[6], George J. Netto[11], Rosa Maria Roperto[4], Alberto Magi[2], Christian Fynbo Christiansen[12], Mario Rotondi[13], Helen Liapis[14], Hans-Joachim Anders[15], Andrea Minervini[6], Maria Rosaria Raspollini[16], Paola Romagnani[1,2,4*].

Affiliations:

[1]Excellence Centre for Research, Transfer and High Education for the development of DE NOVO Therapies (DENOTHE), University of Florence, Florence 50139, Italy.

[2]Department of Experimental and Clinical Biomedical Sciences "Mario Serio", University of Florence, Florence 50139, Italy.

[3]Nephrology, Dialysis and Transplantation Unit, Careggi University Hospital, Florence 50139, Italy.

[4]Nephrology and Dialysis Unit, Meyer Children's University Hospital, Florence 50139, Italy.

[5]Department of Experimental and Clinical Medicine, Section of Internal Medicine, University of Florence, Florence 50139, Italy.

[6]Department of Urology, Careggi Hospital, University of Florence, Florence 50139, Italy.

[7]Department of Urology, Spedali Civili Hospital, University of Brescia, Brescia 25123, Italy.

[8]Department of Urology, University of Turin, San Luigi Gonzaga Hospital, Orbassano, Turin 10043, Italy.

[9]Department of Urology, S. Orsola-Malpighi Hospital, University of Bologna, Bologna 40138, Italy.

[10]Department of Urology, University of Padua, Padua 35122, Italy.

[11]Department of Pathology, University of Alabama at Birmingham, Birmingham, AL 35233, USA.

[12]Department of Clinical Epidemiology, Aarhus University Hospital, Aarhus 8200, Denmark.

[13]Unit of Internal Medicine and Endocrinology, ICS Maugeri I.R.C.C.S., Scientific Institute of Pavia, Pavia 28100, Italy.

[14]Department of Pathology & Immunology, Washington University School of Medicine, Saint Louis, MO 63110[†] and Arkana laboratories, Little Rock, AR 72211, USA.

[15]Division of Nephrology, Medizinische Klinik and Poliklinik IV, Klinikum der LMU München, Munich 80336, Germany.

[16]Histopathology and Molecular Diagnostics, University Hospital Careggi, Florence 50139, Italy.

Contributors: Walter Artibani, Nicola Longo, Vincenzo Mirone, Bernardo Rocco, Claudio Simeone, Riccardo Tellini, Carlo Terrone, Alessandro Volpe, Filiberto Zattoni from the RECORd1 Italian Project.

*Correspondence should be addressed to: Paola Romagnani

Dept. of Experimental and Clinical Biomedical Sciences

University of Florence

Viale Pieraccini 6

50139, Firenze, Italy

Phone: +39-055-2758165

e-mail: paola.romagnani@unifi.it

[†]retired

Abstract

Acute tissue injury causes DNA damage and repair processes involving increased cell mitosis and polyploidization, leading to cell function alterations that may potentially drive cancer development. Here we show that acute kidney injury (AKI) increased the risk for papillary renal cell carcinoma (pRCC) development and tumor relapse in humans as confirmed by data collected from several single center and multicentric studies. Lineage tracing of tubular epithelial cells (TECs) after AKI induction and long-term follow-up in mice showed time-dependent onset of clonal papillary tumors in an adenoma-carcinoma sequence. Among AKI-related pathways, NOTCH1 overexpression in human pRCC associated with worse outcome and was specific for type 2 pRCC. Mice overexpressing NOTCH1 in TECs developed papillary adenomas and type 2 pRCCs, and AKI accelerated this process. Lineage tracing in mice identified single renal progenitors as the cell of origin of papillary tumors. Single-cell RNA sequencing showed that human renal progenitor transcriptome showed similarities to PT1, the putative cell of origin of human pRCC. Furthermore, NOTCH1 overexpression in cultured human renal progenitor cells induced tumor-like 3D growth. Thus, AKI can drive tumorigenesis from local tissue progenitor cells. In particular, we find that AKI promotes the development of pRCC from single progenitors through a classical adenoma-carcinoma sequence.

Introduction

Chronic tissue injury related to toxin exposure or viral infections are proven factors in carcinogenesis (*1*). Whether acute tissue injury and remodeling may promote cancer is purely speculative. Acute tissue injury causes DNA damage and repair involving extensive proliferation of resident stem cell populations (*2*) and/or polyploid genome alterations of differentiated cells (*3*). Both conditions may facilitate cancer development. In addition, repair processes trigger signaling pathways that control cell cycle activation, cell survival, and proliferation, stimulating pathways that drive cancer development (*3, 4*). Here, we examine a putative link between acute kidney injury (AKI) and subsequent cancer development. The kidney provides a unique opportunity to study this possibility, since patients with AKI survive for a long time even when developing end stage renal disease (ESRD) with supportive or renal replacement therapies, such as dialysis and kidney transplantation. In both situations, the native kidneys remain *in situ* and allow assessing tumor rates (*5*).

AKI is a global public health concern resulting in 1.7 million deaths per year (*6*). If not lethal in the acute phase, AKI is largely considered reversible as indicated by resumed urine production or biomarkers assessing injury resolution (*7*). However, even mild AKI episodes give a substantial risk for subsequent chronic kidney disease (CKD) due to irreversible nephron loss (*8*). In this study, we hypothesized that AKI, and particularly ischemia reperfusion injury (IRI), may be a risk factor for one or more types of renal cell carcinoma (RCC), by inducing tissue repair signaling pathways that may drive neoplastic growth.

Results

AKI is associated with RCC in two different human cohorts

To assess the potential role of AKI insults as a risk factor for RCC development, we reviewed the hospital database of the Careggi University Hospital, Florence, Italy for all the patients with incident RCC (n=1618) who underwent surgery between 2012 and 2018 (fig. S1). We retrieved laboratory information for 468 patients with a minimum follow-up of one year before tumor diagnosis. AKI episodes were identified in the patients' clinical history in 76/468 (16.2%), corresponding to an incidence rate estimate of 420 AKI episodes per 10,000 person-years, while the expected rate in the general population is 50 to 150 per 10,000 person-years (*9, 10*). In detail, comparing our population with the one described by Sawhney et al. (*9*) yielded an AKI incidence ratio of 3.2 (95%CI: 2.6-4.1).

To confirm the observed association between AKI episodes and RCC, we analyzed a nationwide cohort study in Denmark (population 5.4 million) using population-based medical databases (*11, 12*). We identified all patients with a hospital diagnosis of AKI between 1977 and 2006 (fig. S2). We obtained data on subsequent incident RCCs and quantified the risk of RCC after AKI. Among 12,480 patients diagnosed with AKI, 7 (0.06%) were diagnosed with RCC within the first year and 14 (0.1%) were diagnosed with RCC more than one year after the first AKI episode. Comparing the observed number of RCC with the expected number computed based on age- and sex-specific cancer incidence rates in the general Danish population (1.6 in the first year and 6.7 cancer cases in the subsequent years) led to calculation of standardized incidence ratios for developing RCC of 4.4 (95%CI: 1.7-9.0) one year after the AKI episode and of 2.1 afterwards (95%CI: 1.1-3.5). These results suggest that AKI episodes associate with RCC.

AKI episodes are a risk factor for pRCC development and recurrence in a single center study

We evaluated whether AKI episodes associated with clear cell RCC (ccRCC) and/or pRCC, the two most frequent tumor histotypes accounting for approximatively 75% and 15% of RCCs, respectively (*13*). We

retrieved clinical and laboratory information for 56 pRCC and 75 ccRCC stage T1 or T2 patients with a minimum follow-up of one year before tumor diagnosis (Table 1, fig. S1). The frequency of the exposure (that is previous AKI episodes) was significantly higher in pRCC patients compared to a cohort of 101 in-house non-tumor controls (21.4% vs. 6.9%, p = 0.008, Table 1). For ccRCC, there was no significant difference (12.0% vs. 6.9%, p = 0.247, Table 1). To further investigate the association with AKI episodes, a binary logistic regression was performed including known risk factors for RCC such as male gender, age, presence of diabetes mellitus (DM), and CKD as covariates (*14*). With multivariate analysis, a previous AKI episode was significantly associated with pRCC development (OR 3.48, 95%CI: 1.14-10.67) compared to controls (Table 1), but there was no significant correlation in ccRCC patients (Table 1). pRCC can be classified into type 1 and type 2 based on histology (56 pRCC patients: 21 type 1, 28 type 2, and 7 undefined). Among the 28 patients affected by type 2 pRCC, 7 had a previous AKI episode (25% vs. 6.9% of controls p=0.012), while out of the 21 type 1 patients, 3 had AKI (14.3% vs. 6.9% p=0.37). The remaining 2 patients with AKI had unclassified pRCC histotype. These findings suggest that AKI could be a risk factor for pRCC development and particularly for the type 2 subtype.

Resection of localized pRCC is frequently associated with postoperative AKI, because of renal artery clamping, parenchymal mass reduction, intraoperative hypotension, and decreased renal perfusion pressure (*15*). We investigated whether AKI upon pRCC surgery could be a risk factor for tumor recurrence. In 83 patients, a follow-up of at least one year after nephrectomy for pRCC (mean follow-up 3.31 years ± 1.84) was available (fig. S1). In this cohort, postoperative AKI occurred in 18/83 (21.7%) patients, similar to previous reports (*16*). While the cumulative recurrence frequency was 14/83 (16.9%), it was significantly more frequent among patients who experienced postoperative AKI compared to non-AKI patients (7/18, 38.9% vs 7/65, 10.8%, p=0.005) (table S1). Five-year recurrence-free survival was significantly (p=0.008) lower in postoperative AKI patients (Fig. 1A). A binary logistic regression was performed to evaluate the association between postoperative AKI and recurrence, including age at

surgery, clinical T stage, and R.E.N.A.L. (radius, exophytic/endophytic properties, nearness of deepest tumor portion to collecting system or sinus, anterior/posterior, and location relative to polar line) nephrometry score, a surgical indicator of tumor complexity previously associated with recurrence (*17*), as covariates. By multivariate analysis, postoperative AKI was significantly associated with recurrence (OR 7.24, 95%CI: 1.65-31.86) (table S1). Taken together, these results suggest that an AKI episode could be a previously unrecognized major risk factor for pRCC recurrence.

A multicentric study confirms that AKI episodes are a risk factor for pRCC recurrence

To validate the association between AKI and pRCC, we analysed The Italian Registry of Conservative Renal Surgery (RECORd1 Project), a 4-year prospective observational multicentric study promoted by the Leading Urological Non-Profit Foundation for Advanced Research (LUNA) of the Italian Society of Urology (*18*). Overall, 769 consecutive patients underwent partial nephrectomy for a renal tumor at 19 Italian urological institutions from 2009 to 2012 (fig. S3). For the current study, we extracted data on 594 patients with a histologic diagnosis of RCC and with a minimum of 1-year follow-up after surgery. Renal function was evaluated at baseline and at 1st postoperative day. Table S2 summarizes the baseline features of the entire cohort.

In 89 patients with pRCC histotype, 18 (20.2%) patients experienced local recurrence, while no systemic recurrences were recorded. Forty-six (51.7%) patients experienced postoperative AKI. In these patients, a significantly higher rate of local recurrence was found (30.4% vs 9.3% in non-AKI patients; p=0.01) (table S3). Survival analysis s showed a significantly (p=0.021) lower 5-year recurrence-free survival in patients experiencing a postoperative AKI episode compared to those without (Fig. 1B). By multivariate analysis, the association between postoperative AKI and tumor recurrence remained significant

(p=0.023) after adjustment for age at surgery and clinical T stage (table S3). Taken together, these results confirm that AKI at surgery is associated with pRCC recurrence.

Long-term follow-up reveals that AKI induces papillary tumors in mice

To experimentally test the hypothesis that AKI promotes tumor development, we induced unilateral ischemia-reperfusion injury (IRI) in wild-type mice and examined their kidneys in the long term at different time points (fig. S4A). Development of type 1 as well as type 2 papillary tumors occurred in a time-dependent manner (Fig. 2, A-H). Over the course of 36 weeks, the lesions were detectable by ultrasound imaging (Fig. 2, A and B). Papillary tumors ranged from small adenomas with low nuclear grade to pRCC appearing as larger papillary tumors with high nuclear grade (Fig. 2, C-F). Type 1 papillary tumors appeared as papillae and tubular structures covered with monolayers of small cells containing basophilic cytoplasm and small, uniform oval nuclei, often forming cysts (Fig. 2C). Type 2 papillary tumors appeared as multilayered papillae covered by large cells with eosinophilic cytoplasm and large spherical nuclei with prominent nucleoli (Fig. 2D) and frequent high nuclear grade (Fig. 2E) as described in the most recent World Health Organization (WHO) pRCC classification (*19*). In addition, focal accumulation of foamy macrophages in the stroma of the papillary stalks (a highly characteristic pRCC finding) was also seen in papillary mouse tumors (Fig. 2F). No tumors were found 4 weeks after AKI, but 55.6% of mice had papillary adenomas at 12 and at 36 weeks (Fig. 2G). At 36 weeks, 22.2% of mice showed pRCC (Fig. 2G). Overall, 68.75% of the tumors were of type 1 and 31.25% of type 2 (Fig. 2H). In contrast, mice that did not undergo IRI did not develop any tumors (fig. S4B). These results suggest that AKI is a risk factor for type 1 and type 2 mouse papillary tumors, similar to findings in humans.

AKI-driven papillary tumors originate from proliferation of single mouse tubular epithelial cells

To study the origin of papillary tumors, we evaluated their clonality using a lineage tracing approach based on the Confetti reporter stochastic labeling of tubular epithelial cells (TECs) at single cell level with different fluorochromes, that is *Pax8.rtTA;TetO.Cre;R26.Confetti* (Pax8/Confetti) mice (fig. S4, C and D). Both type 1 (Fig. 2, I and J) and type 2 (Fig. 2, K and L) papillary tumors tagged at 36 weeks after IRI were mostly of single colors. Indeed, clonal analysis revealed that >95% of type 1 and type 2 papillary tumors were monoclonal (Fig. 2M). Of note, type 1 tumors stained positively for cytokeratin 7 (CK7) (Fig. 2J) while type 2 did not (Fig. 2K), as reported in pRCC patients (*13*). Additionally, type 2 pRCCs presented extensive nuclear atypia, as shown in Fig. 2L. 3D analysis confirmed that clonal populations from the primary tumors invaded the kidney parenchyma (Fig. 2N) and that papillary tumors showed characteristic aberrant vascularization, confirming invasive growth typical of carcinomas (Fig. 2O). Thus, papillary tumors developing after post-ischemic AKI originate from clonal amplification of single TECs.

Human pRCCs associate with altered AKI-activated pathways

To understand how AKI could drive pRCC formation, we speculated that AKI-activated signaling pathways could promote pRCC pathogenesis. To this aim, we analyzed AKI-activated pathways included in the protein array deposited in The Cancer Genome Atlas (TCGA), (https://cancergenome.nih.gov/cancersselected/kidneypapilary) from 161 patients with pRCC (*20*). Among the pathways involved in post-AKI repair (table S4), a decreased expression of mTOR, β-catenin, VHL, and an increased expression of NOTCH1 were associated with advanced pRCC stage (T3-T4) at diagnosis (Fig. 3A). A survival analysis indicated that among them, only increased NOTCH1 associated with worse prognosis (Fig. 3B and table S4). Low amounts of PTEN and SMAD4 also associated with

worse prognosis (Fig. 3, C and D; table S4). Type 1 and type 2 pRCC associated with differences in expression of distinct AKI-related signaling pathways (Fig. 3E). In particular, high amounts of mTOR, β-catenin, and VHL associated with type 1, while high amounts of NOTCH1 strongly associated with type 2 (Fig. 3E). These results suggest that pRCC is associated with altered AKI-activated pathways.

NOTCH1 overexpression is specific for human type 2 pRCC and predicts poor prognosis

NOTCH1 strongly associates with disease severity and patient survival in pRCC, is highly specific for type 2 subtype, and has critical importance in AKI repair (*21*). These specificities prompted us to examine by the Cancer Genome Atlas (TCGA) Research Network data, focusing our attention on NOTCH1 (*20*). The results presented by TCGA Research Network indicate that type 2 pRCC consists of at least three subtypes based on molecular features (clusters C2a, C2b, and C2c-CIMP) (*20*). NOTCH1 protein was increased in all these subgroups, but not in type 1 pRCCs (cluster C1) (Fig. 3F). Type 1 and type 2 pRCCs are both associated with several gene mutations (*20*). Germline or somatic mutations of the tricarboxylic acid cycle enzyme gene fumarate hydratase (*FH*), or the NRF2/antioxidant response element (ARE) pathway, including *CUL3*, *KEAP1*, *NF2*, and *NFE2L2* (NRF2) (*22*), can cause sporadic pRCC that is usually type 2. In contrast, activating germline *MET* mutations cause hereditary type 1 pRCCs (*20*). Type 1 pRCCs with *MET* mutations did not show increased NOTCH1 (Fig. 3G). In contrast, type 2 pRCCs characterized by *CDKN2A* silencing, or by *SETD2BAP1/PBRM1* mutations or by mutations in *FH* or NRF2–ARE pathway (*20*), showed increased NOTCH1 protein in comparison to non-mutated tumors (Fig. 3G). Lifetime survival analysis revealed that NOTCH1 protein amounts correlated with survival in patients with type 2 pRCC (Fig. 3H). Finally, multivariate analysis showed that NOTCH1 expression in tumors correlated with prognosis even when compared to known risk factors for pRCC (table S5). These

results indicate that the AKI-associated pathway Notch1 is a critical prognostic factor for all subgroups of type 2 but not for type 1 pRCC.

NICD1 overexpression in mouse tubular cells drives clonal type 2 papillary tumors

To verify whether NOTCH1 overexpression could trigger type 2 pRCC development, we generated *Pax8.rtTA;TetO.Cre;R26.NICD1.GFP* (Pax8/NICD1) transgenic mice with overexpression of the intracellular portion of the *Notch1* gene (NICD1) in Pax8+ TECs after induction by administration of doxycycline in drinking water (fig. S5A). In order to verify the effective activation of the transgenes and subsequent expression of the NICD1 and GFP proteins, we stained Pax8/NICD1 kidney sections with an anti-GFP antibody. We observed that TECs expressed high amounts of GFP, while interstitial cells remained negative (fig. S5B). We analyzed the animals at weeks 4, 12, and 36 after transgene induction (fig. S5C). Blood urea nitrogen (BUN) measurements revealed a progressive decline of renal excretory function in induced versus uninduced Pax8/NICD1 mice (fig. S5D). Kidney weights and volumes were higher and increased over time in induced Pax8/NICD1 mice (fig. S5, E and F). Histological analysis revealed cystic changes (fig. S5G), with or without epithelial hyperplasia or tumors (fig. S5, H and I). In particular, kidneys of Pax8/NICD1 mice developed numerous papillary tumors in the cortex and outer stripe of the outer medulla at 12 weeks that increased in size, number, and complexity over time (fig. S5, H and I). The uninduced Pax8/NICD1 mice did not develop CKD, renomegaly, or other lesions (fig. S5J).

Notably, animals that were homozygous for the *R26.NICD1.GFP* effector transgene (Pax8/NICD1$^{+/+}$) had significantly more papillary adenomas (pAdenomas)/pRCCs than heterozygotes (Pax8/NICD1$^{+/-}$) at 24-36 weeks (p=0.03 and p=0.005, respectively), suggesting that high NICD1 amounts are critical for generation of papillary tumors (fig. S5K).

All Pax8/NICD1 mice had CKD (fig. S5D) and 93.75% developed papillary tumors at 36 weeks (Fig. 4A), reaching up to 1.6 millimeters in size (Fig. 4B) and detectable by Power Doppler imaging as vascularized masses (Fig. 4C). Interestingly, papillary tumors consisted of both adenomas (Fig. 4D) as well as pRCC (Fig. 4, E and F), but were only type 2 (100% of the tumors). Papillary tumors were negative for carbonic anhydrase IX (CAIX) (Fig. 4G), as reported in human pRCC (*13*). Strong BCL-2 expression was detected, suggesting resistance to cell death (Fig. 4H).

We then evaluated the clonal composition of NOTCH1 overexpression-induced type 2 papillary tumors by generating *Pax8.rtTA;TetO.Cre;R26.NICD1.GFP;R26.Confetti* (Pax8/NICD1/Confetti) mice (fig. S5L). After induction, clonal analysis revealed that over 80% of the papillary tumors in Pax8/NICD1/Confetti mice at 36 weeks were either mono- or biclonal (Fig. 4, I-K, and fig. S5, M-O). 3D analysis confirmed that multiple papillary tumors were interconnected and generated by a clonal population spreading from the primary pRCC and invading the surrounding kidney tissue (Fig. 4L, video S1). Primary tumor masses also showed vascularization (Fig. 4M).

Tumors invading the surrounding kidney tissue or the kidney capsule and/or metastasizing at distant sites were observed in all (100%) mice. Interestingly, metastatis was associated with areas that showed rhabdoid-like morphology, characteristic of high-grade pRCC (*23*), within the dominant pRCC mass (Fig. 4, N and O), as well as in the metastasis (Fig. 4P). Metastases were also positive for PAX2, confirming their renal origin (Fig. 4Q). Cytokeratins (PanCK), vimentin, and epithelial membrane antigen (Mucin 1, cell surface associated (MUC1)) were also expressed, as reported for rhabdoid variants of human RCC metastases (Fig. 4, R-T) (*23*). These results suggest that NOTCH1 overexpression promotes development of papillary adenomas and highly aggressive type 2 pRCCs derived from clonal amplification of single TECs.

AKI accelerates clonal type 2 papillary tumor development in NOTCH1-overexpressing mice

To investigate whether AKI could also act as a tumor-accelerating factor in Pax8/NICD1 mice, we performed unilateral IRI in induced and uninduced Pax8/NICD1 mice (fig. S6A). While activated NOTCH1 expression was virtually absent in uninduced healthy mice (Fig. 5A), IRI alone induced strong NOTCH1 activation in uninduced mice 1 day after injury (Fig. 5B); it remained higher compared to controls thereafter (Fig. 5C). Strong nuclear NOTCH1 immunostaining was seen, indicating diffuse NOTCH1 activation in TECs of Pax8/NICD1 mice (Fig. 5D). AKI increased NOTCH1 in Pax8/NICD1 mice (Fig. 5, E and F). We then checked whether AKI could accelerate pRCC formation when acting together with NICD1 overexpression. Not surprisingly, the combination of IRI and NICD1 overexpression in induced Pax8/NICD1 and Pax8/NICD1/Confetti mice accelerated the formation of cysts, papillary adenomas, CKD (fig. S6B), and pRCCs in just 4 weeks (Fig. 5, G-I, and fig S6, C and D). Papillary RCC included foamy macrophages (Fig. 5G), stained positive for PAX2 (Fig. 5H), similar to human pRCCs, and were mostly of type 2 (Fig. 5J). By contrast, no tumors were observed in uninduced Pax8/NICD1 or Pax8/Confetti mice with AKI (fig. S6, E and F) or in Pax8/NICD1 and Pax8/NICD1/Confetti mice without AKI at 4 weeks (Fig. 5I and fig. S6, G and H). Notably, papillary tumors induced by AKI were clonal (Fig. 5, K and L). 3D analysis confirmed that papillary tumors showed vascularization and clonal population spread from the primary tumors into the surrounding parenchyma (Fig. 5, M and N). These results establish AKI as an accelerating factor for papillary tumors.

Human renal progenitors are transformed by NOTCH1 overexpression

The monoclonality of papillary tumors as well as their association with AKI suggested a possible origin from renal progenitors. We previously reported that renal progenitors consist of a multipotent progenitor population (*24*) characterized by co-expression of CD133 and VCAM1, and a committed tubular

progenitor that is CD133+VCAM1- (*24*). CD133+VCAM1+ cells are localized at the urinary pole of the Bowman's capsule and represent a rare subset of the scattered CD133+ cells localized mostly in proximal tubule (Fig. 6, A and B). To evaluate the contribution of tubular cell subsets to pRCC in humans, we performed immunomagnetic sorting of CD133+ cells, and stained them with the fluorescent label CFDA-SE. We then seeded labeled CD133+ cells in coculture with unlabeled CD133- cells in a ratio of 1:1. After 5 days of culture, the labeled cell population had undergone many cell divisions, becoming more than 98% of cultured cells at day 10 (Fig. 6C). This enrichment of CD133+ cells related to their ~50 fold higher proliferative capacity compared to CD133- cells (Fig. 6D, p=0.00003), as also demonstrated by the high number of cell divisions observed with CFDA-SE labelling (Fig. 6E). Accordingly, overgrown traced cells were virtually all CD133+VCAM1+ (Fig. 6F), in agreement with previous studies (*24*). We then overexpressed NICD1 in primary cultures of human renal progenitors by ZsGreen1-NICD1 lentivirus infection (*25*). In comparison to mock-infected cells (Fig. 6, G and H), NICD1-infected renal progenitors acquired an enlarged, eosinophilic cytoplasm with prominent nucleoli and nuclear grooves (Fig. 6I), typical of pRCC histology (*26*), and a more developed cytoskeleton (Fig. 6J). More importantly, when mock-infected renal progenitors were cultured in a microfluidic device under fluid shear stress, they reconstituted a 3D tubule with a lumen (Fig. 6K), whereas NICD1 overexpression changed the orientation of renal progenitor cell divisions leading to generation of papilla-like structures within the lumen (Fig. 6L) that elongated, filling the lumen and generating tumor-like masses (Fig. 6M).

NOTCH1 overexpression induces renal progenitor proliferation and aberrant mitosis

We next analysed how NOTCH1 overexpression could promote renal progenitor transformation. We previously reported that Notch pathway is active in renal progenitors in culture and controls their proliferation (*25*). Indeed, NICD1-infection further enhanced renal progenitor proliferation (fig. S7A).

Mitoses in mock-infected cultures were normal (fig. S7, B and C), whereas NICD1-infected progenitors frequently showed abnormal mitotic spindle distribution (fig. S7, D and E). These results suggest that NOTCH1 activation induced normal renal progenitor mitosis, whereas NOTCH1 hyperactivation disrupted cell polarity signaling leading to a striking number of aberrant mitoses (fig. S7, B-F). Transcriptome analysis identified numerous genes differentially expressed between NICD1-infected renal and mock-infected progenitor cells (fig. S7G). Gene ontology analysis demonstrated downregulation in NICD1-infected progenitors of several pathways involved in check-points and/or mitotic spindle control, including E2F targets (*27*), G2M checkpoint, and MYC targets V1 and V2 (*28*) (fig. S7H). In particular, several genes that control mitotic spindle polarity, such as *INSC, DYNC2H1, PRKAA2, DLG1, PARD3, PARD6G, STK33, HNF1B,* and *CCNE1* were deregulated (fig. S7I) (*29, 30*). Of note, survival analysis of 285 patients with pRCC from the Human Protein Atlas (*31*) (http://www.proteinatlas.org) showed that the modulation of transcripts of some of these mitotic spindle genes in tumor tissue of patients with pRCCs correlated with reduced survival (fig. S7, J-M). Taken together, NOTCH1 overactivation deregulates the expression of genes controling mitotic spindle polarity and promotes renal progenitor proliferation as well as aberrant mitosis.

Renal progenitors express NOTCH1 after AKI and represent the cell of origin of pRCC in humans

To evaluate NOTCH1 expression in humans after AKI, we analysed biopsies of four patients. Patients with AKI showed nuclear expression of NOTCH1 in 77±4.7% of CD133+ vs. 51.3±6.9% of CD133- tubular cells (Fig. 6, N-O; p=0.03).

Recently, Young et al. (*32*) identified the putative cell of origin of pRCCs using single-cell RNA sequencing (scRNAseq) as a rare VCAM1+ SLC17A3+ SLC7A13- proximal tubular cell. This cell cluster signature was defined as PT1. We then analyzed their pRCC scRNAseq dataset together with

scRNAseq data obtained from wild-type human renal progenitor cell cultures from our laboratory to evaluate if they represented the same population. After correcting for batch effects by matching mutual nearest neighbors (*33*), we reduced dimensionality by running a principal-component analysis (PCA) on the most highly variable genes, performed graph-based clustering on the significant ($p<0.05$) principal components (PCs), and finally visualized distinct cell subgroups using Uniform Manifold Approximation and Projection (UMAP) algorithm. Unsupervised clustering of the entire pooled dataset identified 7 transcriptionally distinct populations (Fig. 6P), 4 deriving from Young's (1, 3, 4, 5) and 3 from our data (0, 2, 6). The pRCC cell cluster 5 characterized by PT1 signature markers clustered together with the renal progenitor cell clusters 0 and 6, which showed a similar pattern of mRNA expression (Fig. 6, Q and R). Importantly, all three clusters expressed *CD133* (*PROM1*) and *PAX2*, as well as the epithelial cell adhesion molecule *EPCAM*, further suggesting that the cell of origin of pRCC corresponded to renal progenitor cells. Taken together, these results suggest that NOTCH1 overexpression may induce pRCC and papillary tumor-like growth from human renal progenitors.

AKI induces papillary tumors by promoting clonal expansion of renal progenitors in mice

To evaluate the role of renal progenitors in pRCCs in vivo, we used *Pax2.rtTA;TetO.Cre* transgenic mice, which specifically track renal progenitors in the mouse kidney, where CD133 cannot be used because it is species-specific (*34*, *35*). For this purpose we generated conditional *Pax2.rtTA;TetO.Cre;R26.NICD1.GFP* (Pax2/NICD1) and *Pax2.rtTA;TetO.Cre;R26.NICD1.GFP; R26.Confetti* (Pax2/NICD1/Confetti) mice (fig. S8A), allowing NICD1 overexpression in the Pax2+ subpopulation of TECs (renal progenitors) and their clonal tracing upon doxycycline induction (fig. S8B), as previously described (*34*, *35*). In order to verify the effective activation of the transgenes, we stained Pax2/NICD1 kidney sections with an anti-GFP antibody (fig. S8C). We observed positive cells in the

Bowman's capsule and scattered in the tubules, consistent with Pax2+ cell distribution (*34, 35*). Four weeks after IRI, more than 85% of induced Pax2/NICD1 mice presented with type 2 papillary tumors that stained positive for BCL-2 (Fig. 7A-E and fig. S8, D and E), similar to those observed in Pax8/NICD1 mice at 4 weeks after IRI (Fig. 5). Most of the papillary lesions were of type 2 (Fig. 7, A-D and F). Histological analysis of uninduced Pax2/NICD1 mice 4 weeks after IRI and Pax2/NICD1 mice without AKI did not show neoplastic lesions (fig. S8, F and G). 3D analysis confirmed papillary tumor vascularization and clonal invasive tumor growth in the surrounding parenchyma (Fig. 7, C and D). Clonal analysis of papillary tumors in Pax2/NICD1/Confetti mice 4 weeks after IRI (Fig. 7, B-D, fig. S8H) revealed that 88% of pAdenomas/pRCCs were monoclonal, the rest being biclonal and triclonal (Fig. 7G). A direct quantitative comparison of type 2 papillary tumors in Pax8/NICD1 and Pax2/NICD1 4 weeks after IRI showed similar numbers of these lesions in both mice (Fig. 7H). In addition, no CKD was seen in Pax2/NICD1 mice after 4 weeks (Fig. 7E and fig. S8I), whereas a large proportion of Pax8/NICD1 mice showed reduced kidney function (Fig. 7E and fig. S6B). To further verify whether the role of AKI in papillary tumor induction relates to endogenous NOTCH1 activation, we induced IRI in Pax2/NICD1/Confetti mice and treated them for one week with N-[N-(3,5-Difluorophenacetyl)-L-alanyl]-S-phenylglycine t-butyl ester (DAPT). In this setting, DAPT blocks only the endogenous AKI-induced Notch1 activation, but not the transgene-derived NICD1. DAPT-treated Pax2/NICD1/Confetti mice developed significantly (p=0.008) fewer papillary tumors, compared to vehicle-treated mice 4 weeks after IRI (Fig. 7I). These results suggest that single renal progenitors are the source of papillary tumors induced by NOTCH1 overexpression.

To address whether clonal tumors developing spontaneously in mice after AKI also originated from renal progenitors, we first confirmed that in Pax2/Confetti mice NOTCH1 was expressed by renal progenitors at a percentage significantly higher than that of Pax2- cells after AKI (p=0.03) and of renal progenitors in healthy mice (p=0.03) (fig. S9A). A representative staining is shown in Fig. 7J. We then performed

lineage tracing for 36 weeks after IRI induction using Pax2/Confetti mice (Fig. 7K-R). Papillary tumors spontaneously developed in Pax2/Confetti mice after IRI (Fig. 7K). As previously observed in Pax8/Confetti mice (Fig. 2M), Pax2/Confetti mice showed a clonal origin (Fig. 7L). Type 1 papillary tumors were prevalent (Fig. 7M). DAPT-treated Pax2/Confetti mice developed significantly (p=0.03) fewer papillary tumors, compared to vehicle-treated mice 4 weeks after IRI (Fig. 7N). This reduction was related to a decrease of type 2 papillary tumors (fig. S9, B and C). 3D analysis confirmed that papillary tumors showed vascularization and that clonal populations spread from the primary tumors into the surrounding parenchyma, promoting invasive clonal tumor growth (Fig. 7, Q and R). These results suggest that papillary tumors that develop after AKI derive from clonal proliferation of single renal progenitors in a Notch-dependent manner.

Discussion

We hypothesized that AKI may drive the development of one or more subtypes of RCC. Our results reveal that: 1. AKI is a risk factor for pRCC development and for pRCC recurrence in humans in different cohorts. 2. AKI promotes long-term development of papillary tumors in mice by activating tumor growth-promoting pathways in a type 1- or 2-specific manner. 3. Overexpression of the AKI-associated pathway Notch1 is a specific feature of type 2 pRCC, which correlates with outcome in humans, and drives type 2 papillary tumors in an inducible mouse model of pRCC. 4. pRCC originates from clonal proliferation of renal progenitors - the cellular source of tubule regeneration upon AKI - in a classical adenoma-carcinoma sequence leading to invasive pRCC growth and even remote metastasis.

AKI, and particularly IRI, is common and often overlooked. In addition, patients with AKI have a reduced life expectancy (*36*), which may explain why the link between AKI and pRCC has remained unrecognized until now (*6*). Autopsy studies suggest that papillary adenomas are common, with a

prevalence ranging from 5 to 10% before the age of 40 and rising to almost 40% above the age of 70 (*37*). In contrast, pRCCs are considerably rarer, with the exception of patients on dialysis or with a kidney transplant, two patient categories at high risk of AKI (*38*, *39*), where prevalence increases up to 100 times, reaching 2-3% (*40*). These epidemiologic data are in line with our findings in mice, where papillary adenomas were observed in over half of the animals 12 weeks after an AKI episode, whereas pRCCs appeared only 36 weeks after AKI and in only 16% of the animals. These results suggest that the adenoma-carcinoma transformation is a stochastic event that develops only in a minority of patients with papillary adenomas and requires long periods of time and likely additional factors to develop. As further evidence that AKI is an important risk factor for pRCC, postoperative AKI episodes also directly increased the risk for pRCC relapse. These results suggest that all patients at high risk for pRCC, that is patients carrying germinal mutations in pRCC-related genes or patients undergoing pRCC surgery, require rigorous measures to prevent AKI episodes. Once AKI has occurred, careful follow-up for pRCC relapse would be required. These findings may be particularly relevant for dialysis patients or patients with kidney transplant in whom pRCC represents an important cause of death (*41*). Our results suggest that this risk may relate to AKI episodes that are inherent to advanced CKD and kidney transplantation (*5*).

How could AKI promote development of pRCC? Our analysis of human tumor samples reported by TCGA study (*20*) showed that some AKI-associated signaling pathways that critically control healing responses to kidney injury are overexpressed in pRCCs and predict tumor severity and patient survival. Notably, type 1 and type 2 pRCCs reveal associations with different pathways, suggesting that these subtypes are promoted by AKI through activation of distinct signaling pathways involved in cell growth control. To verify this hypothesis, we tried to reproduce papillary tumors by overexpressing one of these AKI-associated pathways in mice. We chose to overexpress the Notch1 pathway as a proof of concept because our analysis of patients from TCGA study (*20*) found NOTCH1 overexpression to predict

disease severity and outcome in pRCC and to be a specific feature of all three molecular subgroups of type 2 pRCC independently of causative germline or somatic mutations. In agreement with our hypothesis, NOTCH1 overexpression in TECs induced papillary adenomas and type 2 pRCC development, and blocking NOTCH hyperactivation after AKI prevented their development in mice. Conversely, a previous study showed that knocking out *Notch1* in the kidney epithelium during development can lead to generation of type 1 papillary adenomas at birth (*42*). Consistent with this result, we also found that type 1 papillary tumors had low amounts of NOTCH1 and were not caused by NOTCH overexpression. However, both NOTCH under- and overexpression determine malfunctioning of the mitotic spindle and hyperproliferation (*43*), as also observed in this study. Taken altogether, these results suggest that environmental or genetic factors that promote hypo or hyperactivation of signaling pathways that control tubular cell proliferation, such as the Notch pathway, can drive papillary tumors. Previous studies reported that NOTCH overexpression in TECs promotes CKD, increased proliferation, and even epithelial dysplasia, but not RCC (*44-46*). However, in these studies: 1. mice were studied in the absence of AKI and only 4-8 weeks after transgene activation (*44, 45*), a time that is not sufficient for tumor development, in agreement with our observations; 2. *Notch* transgene was overexpressed under the control of a promoter (*46*) that is not expressed in renal progenitors as previously reported (*47*). Indeed, our results demonstrate that NOTCH1 activation induces RCC only after overexpression specifically in renal progenitors.

Until now, the cell of origin for pRCC has been unknown. Because the renal tubule contains 10 to 20 different epithelial cell subtypes (*48*), not every TEC may be amenable to cancer transformation, making identification of the cell type of pAdenoma/pRCC origin a challenging task. Immunolabeling and mRNA profiling support a possible proximal tubular origin (*49, 50*). Our lineage tracing studies indicate that pAdenoma/pRCC sequentially develop from an aberrant clonal expansion of renal progenitors occurring after AKI or after genetically-induced changes of an AKI-activated pathway specifically in renal

progenitors. These results demonstrate a crucial role of the cell of origin in determining the renal papillary tumor type. Our results also provide a possible explanation for recent results obtained from scRNAseq suggesting the similarity of pRCCs with a scattered, uncharacterized population of tubular cells expressing VCAM1, defined as PT1 (*32*). We previously reported that a subset of CD133+ renal progenitors in humans has self-renewal and clonogenic capacity and is VCAM1+ (*3, 24*). Our scRNAseq analysis indicated that the PT1 signature closely resembled CD133+ human renal progenitor cells, further confirming that this is the cell of origin of pRCC. In this setting, AKI-induced hypoxia may also be critical. Indeed, hypoxia promotes the undifferentiated cell state in various stem and precursor populations by activating Notch-responsive promoters and increasing expression of genes directly downstream of Notch (*51*). In turn, NOTCH also drives a HIF1a-to-HIF2a switch that favors transformation into cancer stem cells and supports tumor growth (*52*).

Our study also has some limitations. In mouse models we tested only IRI, the most frequent type of AKI in clinical settings (*6*). Other studies are needed to determine whether other types of AKI, such as toxic or obstructive, also promote papillary tumor development in animal models. In addition, we did not assess whether the risk of pRCC was related to the severity of AKI. Other studies are needed to address this important point.

In summary, the results of this study provide evidence that acute organ injury can drive tumorigenesis and, in particular, that AKI promotes the development of pRCC from single renal progenitors through a classical adenoma-carcinoma sequence. The process is initiated by overactivation of AKI-associated pathways that promote clonal expansion of renal progenitors as an overshooting healing response. We identify NOTCH1 overexpression as a common pathomechanism of type 2 pRCC formation, suggesting that this pathway could be targeted in this RCC type. Finally, the discovery of AKI as a risk factor for

pRCC development and relapse suggests that pRCCs unrelated to known risk factors may actually relate to previous AKI episodes, requiring AKI prevention and risk stratification programs.

Materials and methods

Study Design

The purpose of this study was to examine the effect of AKI on RCC development and to identify the mechanisms involved in this process. These objectives were addressed by (i) analyzing AKI insults as a risk factor for RCC development in humans, (ii) analyzing the effect of postoperative AKI related to tumor resection in promoting pRCC recurrence in patients, (iii) confirming AKI as a risk factor for pRCC development in mice, and evaluating pRCC clonality, (iv) analyzing the AKI-related pathways that are involved in tumor progression in human pRCC tissues, (v) evaluating the effect of the AKI-related pathway NICD1 on pRCC formation in a transgenic mouse model of pRCC, (vi) evaluating the transforming effect of NICD1 overexpression on human renal progenitors, the critical cell for the response to AKI, (vii) evaluating renal progenitors as the cell of origin of pRCC in NICD1 overexpressing transgenic mouse and/or in response to AKI.

For all clinical studies, all eligible patients from the available observation period were included without previous sample size calculation and were assigned to predefined clinical groups (control/pRCC/ccRCC, AKI/non-AKI) after retrospective clinical adjudication, as per study design.

Single center study We analyzed the incidence of previous AKI episodes in the RCC population irrespectively of the histological diagnosis. All patients who underwent surgery for RCC at the Careggi University Hospital, Florence, Italy, from 2012 to 2018 (fig. S1) with available clinical and laboratory

information and a follow-up of at least one year before tumor diagnosis were included in the analysis. Patients were excluded if no detailed information about the tumor clinical stage was available and in case of TNM stage 3 or 4. Historical clinical records for laboratory, surgical, and histological data of RCC patients were retrospectively and independently collected by two blinded observers. We evaluated the exposure to previous AKI episodes as an independent risk factor for the development of pRCC or ccRCC. AKI that occurred in the 6 months before surgery were excluded from the analysis. When at least one year of follow-up after surgery was available (fig. S1), we evaluated the association between postoperative AKI and tumor recurrence both in a survival analysis and in a multivariate model. This study was approved by the Ethical Committee on Human Experimentation of the Azienda Ospedaliero-Universitaria Careggi, Florence, Italy.

Danish National Registry of Patients A Danish nationwide cohort study using population-based medical databases (*11*, *12*) between 1977 and 2006 was screened for the association between AKI and RCC (fig. S2). All patients diagnosed with AKI were included in the analysis. Data were extracted by an investigator blinded to the purpose of the analysis. The study was approved by the Danish Data Protection Agency (record No 2005-41-5281).

Multicentric study We analyzed the Italian Registry of Conservative Renal Surgery (RECORd1 Project) of the Italian Society of Urology (fig. S3) (*18*) to confirm the association between postoperative AKI and tumor recurrence both in a survival analysis and in a multivariate model. The RECORd project includes all patients who underwent conservative surgical treatment for radiologically diagnosed renal cell carcinoma (RCC) between January 2009 and December 2012 at 19 urological Italian Centres. We included all patients with a histologic diagnosis of RCC and with a minimum 1-year oncologic follow-up (fig. S3). Patients were excluded if no detailed information about the tumor clinical stage was available and in case of TNM stage 3 or 4. Data were extracted by an investigator blinded to the purpose of the

analysis. The study protocol was approved by the local ethical committee and patients' acceptance of the written informed consent .

Cancer Genome Atlas Research Network We analyzed gender, age, smoking exposure, and mutations on genes previously described as specific for pRCC in relation to expression of NOTCH1 and other pathways associated with AKI (*20*) in all availale pRCC patients.

Patient dataset from Human Protein Atlas We analysed the survival probability of all pRCC patients from The Human Protein Atlas (*31*), (http://www.proteinatlas.org) based on PRKAA2, PARD6G, HNF1B, and CCNE1 expression.

Patient biopsies A total of 5 normal-appearing kidneys (3 men and 2 woman, mean age 64.8 ± 12.4 years) and 4 kidney biopsies from patients with AKI (2 men and 2 women, mean age 58.8 ± 5.1 years, time post-AKI: 2, 2, 14, and 15 days) were analyzed in agreement with the Ethical Committee on Human Experimentation of the Azienda Ospedaliero-Universitaria Careggi, Florence, Italy. Normal-appearing kidney fragments were obtained from the pole opposite to the tumor of patients who underwent nephrectomy for localized renal tumors.

Animal studies Mice were randomly assigned to experimental and control groups, but investigators were not blinded. Sample size was calculated based on the primary endpoint rate of tumor formation and other assumptions based on preliminary experiments. No data were excluded from studies in this manuscript. Pathology analysis was performed in a blinded fashion. All procedures were performed in accordance with institutional protocols approved by the Institutional Animal Care and Use Committee of the University of Florence, Italy.

Statistical analysis

Human studies Results are reported as mean±SD unless otherwise stated. Between-group comparisons for continuous variables were performed by Student's t test for unpaired data and Mann–Whitney *U* test according to a normal or non-parametric distribution. Frequencies among groups were compared by chi-squared ($\chi 2$) test for categorical variables, applying Fisher's exact test when appropriate (Table 1 and tables S1-S3). A two-sided p-value of <0.05 was considered statistically significant.

To test the association between previous AKI episodes and postoperative AKI with pRCC development and recurrence, respectively, binary logistic regression models were constructed. pRCC or ccRCC development and pRCC recurrence served as outcome or dependent variables. Covariates or explanatory variables were treated as categorical (AKI, gender, CKD, DM, clinical T) or continuous (age, R.E.N.A.L. score) as appropriate. The results are presented as odds ratio and 95% confidence interval. A Wald test statistics' p-value of <0.05 was considered statistically significant. For survival analyses, Kaplan-Meier estimates for postoperative AKI and non-AKI patients were compared by log-rank test with statistical significance set for a p-value lower than 0.05. Cumulative 4-year recurrence-free survival and standard error are reported.

Kaplan-Meier estimates were used to generate overall survival curves for:

1. NOTCH1, PTEN, and SMAD4 RPPA amounts in patients affected by pRCC, or NOTCH1 (using 50th percentile as a cutoff value) in patients affected by type 1 or 2 pRCC obtained from RPPA data from the Cancer Genome Atlas Research Network (*20*).

2. PRKAA2, PARD6G, HNF1B, and CCNE1 expression (using best expression cut off) in patients affected by pRCC from Human Protein Atlas (*31*).

Differences between groups were assessed by log-rank test. For each Kaplan-Meier plot, a Cox regression model was constructed to provide hazard ratio (HR) and 95% confidence interval.

To test the independent effects of different variables on the prognosis of pRCC, a multiple logistic regression model was constructed by entering TNM stages >2 as dependent variable while all parameters previously described as risk factors for pRCC served as covariates.

Animal and in vitro studies The number of mice used, numbers of replicates, and statistical values (where applicable) are provided in the figure legends. Results were expressed as mean±SEM. Comparison between groups was performed by the Mann-Whitney test, or through the analysis of variance for multiple comparisons (ANOVA for repeated measures) with Bonferroni post hoc analysis, with the Fisher's exact test (two-tailed p-value) or with t-test (two-tailed p-value). A p-value < 0.05 was considered statistically significant.

Statistical analysis was performed using SPSS (RRID:SCR_002865), OriginPro (RRID:SCR_015636), and Stata (RRID:SCR_012763) statistical softwares.

Supplementary Materials

Supplementary Materials and Methods

Fig. S1. The flow chart illustrates the selection criteria for the single center study population.

Fig. S2. The flow chart illustrates the selection criteria for the study population from the Danish National Registry of Patients.

Fig. S3. The flow chart illustrates the selection criteria for the multicentric study population.

Fig. S4. AKI-driven papillary tumors originate from clonal proliferation of single tubular epithelial cells in mice.

Fig. S5. NICD1 overexpression in mouse tubular cells induces papillary tumors and CKD.

Fig. S6. AKI accelerates clonal type 2 papillary tumor development in mice.

Fig. S7. NOTCH1 overexpression enhances cell division and promotes aberrant mitosis.

Fig. S8. AKI induces papillary tumors by promoting clonal expansion of renal progenitors in mice.

Fig. S9. AKI induces papillary tumors from renal progenitors in a NOTCH1-dependent manner.

Table S1. Postoperative AKI is a risk factor for the development of pRCC recurrence in humans in a single center study.

Table S2. The preoperative characteristics of 594 patients treated with partial nephrectomy for kidney tumors and clinical details of 89 pRCC patients (the RECORd1 project).

Table S3. Postoperative AKI is a risk factor for the development of pRCC recurrence in humans in a multicentric study (RECORd1 project).

Table S4. AKI-activated pathways are overexpressed in human pRCC in a subtype-specific manner.

Table S5. Multivariate analysis indicates NOTCH1 as a risk factor for pRCC prognosis.

Video S1. 3D reconstruction of a papillary tumor in Pax8/NICD1/Confetti kidney at 36 weeks

References and notes

1. C. de Martel, S. Franceschi, Infections and cancer: established associations and new hypotheses. *Crit Rev Oncol Hematol* **70**, 183-194 (2009).
2. J. E. Visvader, H. Clevers, Tissue-specific designs of stem cell hierarchies. *Nat Cell Biol* **18**, 349-355 (2016).
3. E. Lazzeri, M. L. Angelotti, C. Conte, H. J. Anders, P. Romagnani, Surviving Acute Organ Failure: Cell Polyploidization and Progenitor Proliferation. *Trends Mol Med* **25**, 366-381 (2019).
4. A. Gregorieff, J. L. Wrana, Hippo signalling in intestinal regeneration and cancer. *Curr Opin Cell Biol* **48**, 17-25 (2017).
5. S. A. Birkeland, H. Lokkegaard, H. H. Storm, Cancer risk in patients on dialysis and after renal transplantation. *Lancet* **355**, 1886-1887 (2000).
6. R. Bellomo, J. A. Kellum, C. Ronco, Acute kidney injury. *Lancet* **380**, 756-766 (2012).
7. N. H. Lameire, A. Bagga, D. Cruz, J. De Maeseneer, Z. Endre, J. A. Kellum, K. D. Liu, R. L. Mehta, N. Pannu, W. Van Biesen, R. Vanholder, Acute kidney injury: an increasing global concern. *Lancet* **382**, 170-179 (2013).
8. M. A. Venkatachalam, J. M. Weinberg, W. Kriz, A. K. Bidani, Failed Tubule Recovery, AKI-CKD Transition, and Kidney Disease Progression. *J Am Soc Nephrol* **26**, 1765-1776 (2015).
9. S. Sawhney, H. A. Robinson, S. N. van der Veer, H. O. Hounkpatin, T. M. Scale, J. A. Chess, N. Peek, A. Marks, G. I. Davies, P. Fraccaro, M. J. Johnson, R. A. Lyons, D. Nitsch, P. J. Roderick, N. Halbesma, E. Miller-Hodges, C. Black, S. Fraser, Acute kidney injury in the UK: a replication cohort study of the variation across three regional populations. *BMJ Open* **8**, e019435 (2018).
10. E. D. Siew, A. Davenport, The growth of acute kidney injury: a rising tide or just closer attention to detail? *Kidney Int* **87**, 46-61 (2015).
11. M. Schmidt, S. A. Schmidt, J. L. Sandegaard, V. Ehrenstein, L. Pedersen, H. T. Sorensen, The Danish National Patient Registry: a review of content, data quality, and research potential. *Clin Epidemiol* **7**, 449-490 (2015).
12. M. L. Gjerstorff, The Danish Cancer Registry. *Scand J Public Health* **39**, 42-45 (2011).
13. H. A. Alshenawy, Immunohistochemical panel for differentiating renal cell carcinoma with clear and papillary features. *J Microsc Ultrastruct* **3**, 68-74 (2015).
14. W. H. Chow, L. M. Dong, S. S. Devesa, Epidemiology and risk factors for kidney cancer. *Nat Rev Urol* **7**, 245-257 (2010).
15. H. D. Patel, P. M. Pierorazio, M. H. Johnson, R. Sharma, E. Iyoha, M. E. Allaf, E. B. Bass, S. M. Sozio, Renal Functional Outcomes after Surgery, Ablation, and Active Surveillance of Localized Renal Tumors: A Systematic Review and Meta-Analysis. *Clin J Am Soc Nephrol* **12**, 1057-1069 (2017).
16. C. F. Christiansen, M. B. Johansen, W. J. Langeberg, J. P. Fryzek, H. T. Sorensen, Incidence of acute kidney injury in cancer patients: a Danish population-based cohort study. *Eur J Intern Med* **22**, 399-406 (2011).
17. A. Nagahara, M. Uemura, A. Kawashima, T. Ujike, K. Fujita, Y. Miyagawa, N. Nonomura, R.E.N.A.L. nephrometry score predicts postoperative recurrence of localized renal cell carcinoma treated by radical nephrectomy. *Int J Clin Oncol* **21**, 367-372 (2016).
18. A. Antonelli, A. Mari, N. Longo, G. Novara, F. Porpiglia, R. Schiavina, V. Ficarra, M. Carini, A. Minervini, Collaborators, Role of Clinical and Surgical Factors for the Prediction of Immediate, Early and Late Functional Results, and its Relationship with Cardiovascular Outcome after Partial Nephrectomy: Results from the Prospective Multicenter RECORd 1 Project. *J Urol* **199**, 927-932 (2018).
19. H. Moch, A. L. Cubilla, P. A. Humphrey, V. E. Reuter, T. M. Ulbright, The 2016 WHO Classification of Tumours of the Urinary System and Male Genital Organs-Part A: Renal, Penile, and Testicular Tumours. *Eur Urol* **70**, 93-105 (2016).

20. N. Cancer Genome Atlas Research, W. M. Linehan, P. T. Spellman, C. J. Ricketts, C. J. Creighton, S. S. Fei, C. Davis, D. A. Wheeler, B. A. Murray, L. Schmidt, C. D. Vocke, M. Peto, A. A. Al Mamun, E. Shinbrot, A. Sethi, S. Brooks, W. K. Rathmell, A. N. Brooks, K. A. Hoadley, A. G. Robertson, D. Brooks, R. Bowlby, S. Sadeghi, H. Shen, D. J. Weisenberger, M. Bootwalla, S. B. Baylin, P. W. Laird, A. D. Cherniack, G. Saksena, S. Haake, J. Li, H. Liang, Y. Lu, G. B. Mills, R. Akbani, M. D. Leiserson, B. J. Raphael, P. Anur, D. Bottaro, L. Albiges, N. Barnabas, T. K. Choueiri, B. Czerniak, A. K. Godwin, A. A. Hakimi, T. H. Ho, J. Hsieh, M. Ittmann, W. Y. Kim, B. Krishnan, M. J. Merino, K. R. Mills Shaw, V. E. Reuter, E. Reznik, C. S. Shelley, B. Shuch, S. Signoretti, R. Srinivasan, P. Tamboli, G. Thomas, S. Tickoo, K. Burnett, D. Crain, J. Gardner, K. Lau, D. Mallery, S. Morris, J. D. Paulauskis, R. J. Penny, C. Shelton, W. T. Shelton, M. Sherman, E. Thompson, P. Yena, M. T. Avedon, J. Bowen, J. M. Gastier-Foster, M. Gerken, K. M. Leraas, T. M. Lichtenberg, N. C. Ramirez, T. Santos, L. Wise, E. Zmuda, J. A. Demchok, I. Felau, C. M. Hutter, M. Sheth, H. J. Sofia, R. Tarnuzzer, Z. Wang, L. Yang, J. C. Zenklusen, J. Zhang, B. Ayala, J. Baboud, S. Chudamani, J. Liu, L. Lolla, R. Naresh, T. Pihl, Q. Sun, Y. Wan, Y. Wu, A. Ally, M. Balasundaram, S. Balu, R. Beroukhim, T. Bodenheimer, C. Buhay, Y. S. Butterfield, R. Carlsen, S. L. Carter, H. Chao, E. Chuah, A. Clarke, K. R. Covington, M. Dahdouli, N. Dewal, N. Dhalla, H. V. Doddapaneni, J. A. Drummond, S. B. Gabriel, R. A. Gibbs, R. Guin, W. Hale, A. Hawes, D. N. Hayes, R. A. Holt, A. P. Hoyle, S. R. Jefferys, S. J. Jones, C. D. Jones, D. Kalra, C. Kovar, L. Lewis, J. Li, Y. Ma, M. A. Marra, M. Mayo, S. Meng, M. Meyerson, P. A. Mieczkowski, R. A. Moore, D. Morton, L. E. Mose, A. J. Mungall, D. Muzny, J. S. Parker, C. M. Perou, J. Roach, J. E. Schein, S. E. Schumacher, Y. Shi, J. V. Simons, P. Sipahimalani, T. Skelly, M. G. Soloway, C. Sougnez, A. Tam, D. Tan, N. Thiessen, U. Veluvolu, M. Wang, M. D. Wilkerson, T. Wong, J. Wu, L. Xi, J. Zhou, J. Bedford, F. Chen, Y. Fu, M. Gerstein, D. Haussler, K. Kasaian, P. Lai, S. Ling, A. Radenbaugh, D. Van Den Berg, J. N. Weinstein, J. Zhu, M. Albert, I. Alexopoulou, J. J. Andersen, J. T. Auman, J. Bartlett, S. Bastacky, J. Bergsten, M. L. Blute, L. Boice, R. J. Bollag, J. Boyd, E. Castle, Y. B. Chen, J. C. Cheville, E. Curley, B. Davies, A. DeVolk, R. Dhir, L. Dike, J. Eckman, J. Engel, J. Harr, R. Hrebinko, M. Huang, L. Huelsenbeck-Dill, M. Iacocca, B. Jacobs, M. Lobis, J. K. Maranchie, S. McMeekin, J. Myers, J. Nelson, J. Parfitt, A. Parwani, N. Petrelli, B. Rabeno, S. Roy, A. L. Salner, J. Slaton, M. Stanton, R. H. Thompson, L. Thorne, K. Tucker, P. M. Weinberger, C. Winemiller, L. A. Zach, R. Zuna, Comprehensive Molecular Characterization of Papillary Renal-Cell Carcinoma. *N Engl J Med* **374**, 135-145 (2016).
21. Y. Sirin, K. Susztak, Notch in the kidney: development and disease. *J Pathol* **226**, 394-403 (2012).
22. B. N. Chorley, M. R. Campbell, X. Wang, M. Karaca, D. Sambandan, F. Bangura, P. Xue, J. Pi, S. R. Kleeberger, D. A. Bell, Identification of novel NRF2-regulated genes by ChIP-Seq: influence on retinoid X receptor alpha. *Nucleic Acids Res* **40**, 7416-7429 (2012).
23. N. Gokden, O. Nappi, P. E. Swanson, J. D. Pfeifer, R. T. Vollmer, M. R. Wick, P. A. Humphrey, Renal cell carcinoma with rhabdoid features. *Am J Surg Pathol* **24**, 1329-1338 (2000).
24. M. L. Angelotti, E. Ronconi, L. Ballerini, A. Peired, B. Mazzinghi, C. Sagrinati, E. Parente, M. Gacci, M. Carini, M. Rotondi, A. B. Fogo, E. Lazzeri, L. Lasagni, P. Romagnani, Characterization of renal progenitors committed toward tubular lineage and their regenerative potential in renal tubular injury. *Stem Cells* **30**, 1714-1725 (2012).
25. L. Lasagni, L. Ballerini, M. L. Angelotti, E. Parente, C. Sagrinati, B. Mazzinghi, A. Peired, E. Ronconi, F. Becherucci, D. Bani, M. Gacci, M. Carini, E. Lazzeri, P. Romagnani, Notch activation differentially regulates renal progenitors proliferation and differentiation toward the podocyte lineage in glomerular disorders. *Stem Cells* **28**, 1674-1685 (2010).
26. S. R. Granter, A. R. Perez-Atayde, A. A. Renshaw, Cytologic analysis of papillary renal cell carcinoma. *Cancer* **84**, 303-308 (1998).
27. L. N. Kent, G. Leone, The broken cycle: E2F dysfunction in cancer. *Nat Rev Cancer* **19**, 326-338 (2019).
28. C. Topham, A. Tighe, P. Ly, A. Bennett, O. Sloss, L. Nelson, R. A. Ridgway, D. Huels, S. Littler, C. Schandl, Y. Sun, B. Bechi, D. J. Procter, O. J. Sansom, D. W. Cleveland, S. S. Taylor, MYC Is a Major Determinant of Mitotic Cell Fate. *Cancer Cell* **28**, 129-140 (2015).

29. M. Dias Gomes, S. Letzian, M. Saynisch, S. Iden, Polarity signaling ensures epidermal homeostasis by coupling cellular mechanics and genomic integrity. *Nat Commun* **10**, 3362 (2019).
30. F. Martin-Belmonte, M. Perez-Moreno, Epithelial cell polarity, stem cells and cancer. *Nat Rev Cancer* **12**, 23-38 (2011).
31. M. Uhlen, L. Fagerberg, B. M. Hallstrom, C. Lindskog, P. Oksvold, A. Mardinoglu, A. Sivertsson, C. Kampf, E. Sjostedt, A. Asplund, I. Olsson, K. Edlund, E. Lundberg, S. Navani, C. A. Szigyarto, J. Odeberg, D. Djureinovic, J. O. Takanen, S. Hober, T. Alm, P. H. Edqvist, H. Berling, H. Tegel, J. Mulder, J. Rockberg, P. Nilsson, J. M. Schwenk, M. Hamsten, K. von Feilitzen, M. Forsberg, L. Persson, F. Johansson, M. Zwahlen, G. von Heijne, J. Nielsen, F. Ponten, Proteomics. Tissue-based map of the human proteome. *Science* **347**, 1260419 (2015).
32. M. D. Young, T. J. Mitchell, F. A. Vieira Braga, M. G. B. Tran, B. J. Stewart, J. R. Ferdinand, G. Collord, R. A. Botting, D. M. Popescu, K. W. Loudon, R. Vento-Tormo, E. Stephenson, A. Cagan, S. J. Farndon, M. Del Castillo Velasco-Herrera, C. Guzzo, N. Richoz, L. Mamanova, T. Aho, J. N. Armitage, A. C. P. Riddick, I. Mushtaq, S. Farrell, D. Rampling, J. Nicholson, A. Filby, J. Burge, S. Lisgo, P. H. Maxwell, S. Lindsay, A. Y. Warren, G. D. Stewart, N. Sebire, N. Coleman, M. Haniffa, S. A. Teichmann, M. Clatworthy, S. Behjati, Single-cell transcriptomes from human kidneys reveal the cellular identity of renal tumors. *Science* **361**, 594-599 (2018).
33. L. Haghverdi, A. T. L. Lun, M. D. Morgan, J. C. Marioni, Batch effects in single-cell RNA-sequencing data are corrected by matching mutual nearest neighbors. *Nature Biotechnology* **36**, 421-+ (2018).
34. E. Lazzeri, M. L. Angelotti, A. Peired, C. Conte, J. A. Marschner, L. Maggi, B. Mazzinghi, D. Lombardi, M. E. Melica, S. Nardi, E. Ronconi, A. Sisti, G. Antonelli, F. Becherucci, L. De Chiara, R. R. Guevara, A. Burger, B. Schaefer, F. Annunziato, H. J. Anders, L. Lasagni, P. Romagnani, Endocycle-related tubular cell hypertrophy and progenitor proliferation recover renal function after acute kidney injury. *Nat Commun* **9**, 1344 (2018).
35. L. Lasagni, M. L. Angelotti, E. Ronconi, D. Lombardi, S. Nardi, A. Peired, F. Becherucci, B. Mazzinghi, A. Sisti, S. Romoli, A. Burger, B. Schaefer, A. Buccoliero, E. Lazzeri, P. Romagnani, Podocyte Regeneration Driven by Renal Progenitors Determines Glomerular Disease Remission and Can Be Pharmacologically Enhanced. *Stem Cell Reports* **5**, 248-263 (2015).
36. E. A. Hoste, G. Clermont, A. Kersten, R. Venkataraman, D. C. Angus, D. De Bacquer, J. A. Kellum, RIFLE criteria for acute kidney injury are associated with hospital mortality in critically ill patients: a cohort analysis. *Crit Care* **10**, R73 (2006).
37. *World Health Organization classification of tumors: pathology and genetics of tumors of the urinary system and male genital organs*. (IARC Press, Lyon, France, 2004).
38. B. G. Abu Jawdeh, A. Govil, Acute Kidney Injury in Transplant Setting: Differential Diagnosis and Impact on Health and Health Care. *Adv Chronic Kidney Dis* **24**, 228-232 (2017).
39. L. S. Chawla, P. W. Eggers, R. A. Star, P. L. Kimmel, Acute kidney injury and chronic kidney disease as interconnected syndromes. *N Engl J Med* **371**, 58-66 (2014).
40. M. Gigante, Y. Neuzillet, J. J. Patard, X. Tillou, R. Thuret, J. Branchereau, M. O. Timsit, N. Terrier, J. M. Boutin, F. Sallusto, G. Karam, B. Barrou, D. Chevallier, C. R. Mazzola, V. Delaporte, A. Doeffler, F. Kleinclauss, L. Badet, d. U. members of the Comite de Cancerologie de l'Association Francaise, d. U. Comite de Transplantation de l'Association Francaise, Renal cell carcinoma (RCC) arising in native kidneys of dialyzed and transplant patients: are they different entities? *BJU Int* **110**, E570-573 (2012).
41. T. Klatte, M. Marberger, Renal cell carcinoma of native kidneys in renal transplant patients. *Curr Opin Urol* **21**, 376-379 (2011).
42. K. Surendran, M. Selassie, H. Liapis, H. Krigman, R. Kopan, Reduced Notch signaling leads to renal cysts and papillary microadenomas. *J Am Soc Nephrol* **21**, 819-832 (2010).
43. J. L. Regan, T. Sourisseau, K. Soady, H. Kendrick, A. McCarthy, C. Tang, K. Brennan, S. Linardopoulos, D. E. White, M. J. Smalley, Aurora A kinase regulates mammary epithelial cell fate by determining mitotic spindle orientation in a Notch-dependent manner. *Cell Rep* **4**, 110-123 (2013).

44. T. D. Bhagat, Y. Zou, S. Huang, J. Park, M. B. Palmer, C. Hu, W. Li, N. Shenoy, O. Giricz, G. Choudhary, Y. Yu, Y. A. Ko, M. C. Izquierdo, A. S. Park, N. Vallumsetla, R. Laurence, R. Lopez, M. Suzuki, J. Pullman, J. Kaner, B. Gartrell, A. A. Hakimi, J. M. Greally, B. Patel, K. Benhadji, K. Pradhan, A. Verma, K. Susztak, Notch Pathway Is Activated via Genetic and Epigenetic Alterations and Is a Therapeutic Target in Clear Cell Renal Cancer. *J Biol Chem* **292**, 837-846 (2017).
45. B. Bielesz, Y. Sirin, H. Si, T. Niranjan, A. Gruenwald, S. Ahn, H. Kato, J. Pullman, M. Gessler, V. H. Haase, K. Susztak, Epithelial Notch signaling regulates interstitial fibrosis development in the kidneys of mice and humans. *J Clin Invest* **120**, 4040-4054 (2010).
46. I. Sorensen-Zender, S. Rong, N. Susnik, S. Zender, P. Pennekamp, A. Melk, H. Haller, R. Schmitt, Renal tubular Notch signaling triggers a prosenescent state after acute kidney injury. *Am J Physiol Renal Physiol* **306**, F907-915 (2014).
47. C. Sagrinati, G. S. Netti, B. Mazzinghi, E. Lazzeri, F. Liotta, F. Frosali, E. Ronconi, C. Meini, M. Gacci, R. Squecco, M. Carini, L. Gesualdo, F. Francini, E. Maggi, F. Annunziato, L. Lasagni, M. Serio, S. Romagnani, P. Romagnani, Isolation and characterization of multipotent progenitor cells from the Bowman's capsule of adult human kidneys. *J Am Soc Nephrol* **17**, 2443-2456 (2006).
48. J. Park, R. Shrestha, C. Qiu, A. Kondo, S. Huang, M. Werth, M. Li, J. Barasch, K. Susztak, Single-cell transcriptomics of the mouse kidney reveals potential cellular targets of kidney disease. *Science* **360**, 758-763 (2018).
49. D. Lindgren, P. Eriksson, K. Krawczyk, H. Nilsson, J. Hansson, S. Veerla, J. Sjolund, M. Hoglund, M. E. Johansson, H. Axelson, Cell-Type-Specific Gene Programs of the Normal Human Nephron Define Kidney Cancer Subtypes. *Cell Rep* **20**, 1476-1489 (2017).
50. D. Lindgren, A. K. Bostrom, K. Nilsson, J. Hansson, J. Sjolund, C. Moller, K. Jirstrom, E. Nilsson, G. Landberg, H. Axelson, M. E. Johansson, Isolation and characterization of progenitor-like cells from human renal proximal tubules. *Am J Pathol* **178**, 828-837 (2011).
51. M. V. Gustafsson, X. Zheng, T. Pereira, K. Gradin, S. Jin, J. Lundkvist, J. L. Ruas, L. Poellinger, U. Lendahl, M. Bondesson, Hypoxia requires notch signaling to maintain the undifferentiated cell state. *Dev Cell* **9**, 617-628 (2005).
52. A. P. Mutvei, S. K. Landor, R. Fox, E. B. Braune, Y. L. Tsoi, Y. P. Phoon, C. Sahlgren, J. Hartman, J. Bergh, S. Jin, U. Lendahl, Notch signaling promotes a HIF2alpha-driven hypoxic response in multiple tumor cell types. *Oncogene* **37**, 6083-6095 (2018).
53. P. Mouracade, O. Kara, M. J. Maurice, J. Dagenais, E. Malkoc, R. J. Nelson, J. H. Kaouk, Patterns and Predictors of Recurrence after Partial Nephrectomy for Kidney Tumors. *J Urol* **197**, 1403-1409 (2017).
54. Kidney Disease: Improving Global Outcomes (KDIGO) CKD Work Group. KDIGO 2012 clinical practice guideline for the evaluation and management of chronic kidney disease. *Kidney Int Suppl* **3**, 1-150 (2013).
55. KDIGO AKI Work Group. KDIGO clinical practice guideline for acute kidney injury. *Kidney Int Suppl* **17**, 1-138 (2012).
56. K. M. Park, J. I. Kim, Y. Ahn, A. J. Bonventre, J. V. Bonventre, Testosterone is responsible for enhanced susceptibility of males to ischemic renal injury. *J Biol Chem* **279**, 52282-52292 (2004).
57. E. Higashihara, K. Nutahara, T. Okegawa, M. Tanbo, H. Hara, I. Miyazaki, K. Kobayasi, T. Nitatori, Kidney volume estimations with ellipsoid equations by magnetic resonance imaging in autosomal dominant polycystic kidney disease. *Nephron* **129**, 253-262 (2015).
58. J. M. Shillingford, N. S. Murcia, C. H. Larson, S. H. Low, R. Hedgepeth, N. Brown, C. A. Flask, A. C. Novick, D. A. Goldfarb, A. Kramer-Zucker, G. Walz, K. B. Piontek, G. G. Germino, T. Weimbs, The mTOR pathway is regulated by polycystin-1, and its inhibition reverses renal cystogenesis in polycystic kidney disease. *Proc Natl Acad Sci U S A* **103**, 5466-5471 (2006).
59. D. Nguyen, Quantifying chromogen intensity in immunohistochemistry via reciprocal intensity. (2013).
60. G. Chen, X. Deng, Cell Synchronization by Double Thymidine Block. *Bio Protoc* **8**, (2018).

61. A. Subramanian, P. Tamayo, V. K. Mootha, S. Mukherjee, B. L. Ebert, M. A. Gillette, A. Paulovich, S. L. Pomeroy, T. R. Golub, E. S. Lander, J. P. Mesirov, Gene set enrichment analysis: a knowledge-based approach for interpreting genome-wide expression profiles. *Proc Natl Acad Sci U S A* **102**, 15545-15550 (2005).
62. A. Liberzon, C. Birger, H. Thorvaldsdottir, M. Ghandi, J. P. Mesirov, P. Tamayo, The Molecular Signatures Database (MSigDB) hallmark gene set collection. *Cell Syst* **1**, 417-425 (2015).
63. A. Dobin, C. A. Davis, F. Schlesinger, J. Drenkow, C. Zaleski, S. Jha, P. Batut, M. Chaisson, T. R. Gingeras, STAR: ultrafast universal RNA-seq aligner. *Bioinformatics* **29**, 15-21 (2013).
64. A. T. L. Lun, K. Bach, J. C. Marioni, Pooling across cells to normalize single-cell RNA sequencing data with many zero counts. *Genome Biology* **17**, (2016).
65. E. Becht, L. McInnes, J. Healy, C. A. Dutertre, I. W. H. Kwok, L. G. Ng, F. Ginhoux, E. W. Newell, Dimensionality reduction for visualizing single-cell data using UMAP. *Nature Biotechnology* **37**, 38-+ (2019).
66. D. Zhou, R. J. Tan, L. Lin, L. Zhou, Y. Liu, Activation of hepatocyte growth factor receptor, c-met, in renal tubules is required for renoprotection after acute kidney injury. *Kidney Int* **84**, 509-520 (2013).
67. J. Li, Z. Xu, L. Jiang, J. Mao, Z. Zeng, L. Fang, W. He, W. Yuan, J. Yang, C. Dai, Rictor/mTORC2 protects against cisplatin-induced tubular cell death and acute kidney injury. *Kidney Int* **86**, 86-102 (2014).
68. J. Chen, H. You, Y. Li, Y. Xu, Q. He, R. C. Harris, EGF Receptor-Dependent YAP Activation Is Important for Renal Recovery from AKI. *J Am Soc Nephrol* **29**, 2372-2385 (2018).
69. M. Yan, C. Tang, Z. Ma, S. Huang, Z. Dong, DNA damage response in nephrotoxic and ischemic kidney injury. *Toxicol Appl Pharmacol* **313**, 104-108 (2016).
70. D. Zhou, Y. Li, L. Lin, L. Zhou, P. Igarashi, Y. Liu, Tubule-specific ablation of endogenous beta-catenin aggravates acute kidney injury in mice. *Kidney Int* **82**, 537-547 (2012).
71. S. Bengatta, C. Arnould, E. Letavernier, M. Monge, H. M. de Preneuf, Z. Werb, P. Ronco, B. Lelongt, MMP9 and SCF protect from apoptosis in acute kidney injury. *J Am Soc Nephrol* **20**, 787-797 (2009).
72. H. Zhou, A. Kato, H. Yasuda, T. Miyaji, Y. Fujigaki, T. Yamamoto, K. Yonemura, A. Hishida, The induction of cell cycle regulatory and DNA repair proteins in cisplatin-induced acute renal failure. *Toxicol Appl Pharmacol* **200**, 111-120 (2004).
73. M. Weidenbusch, S. Rodler, S. Song, S. Romoli, J. A. Marschner, F. Kraft, A. Holderied, S. Kumar, S. R. Mulay, M. Honarpisheh, S. Kumar Devarapu, M. Lech, H. J. Anders, Gene expression profiling of the Notch-AhR-IL22 axis at homeostasis and in response to tissue injury. *Biosci Rep* **37**, (2017).
74. D. Thomasova, M. Ebrahim, K. Fleckinger, M. Li, J. Molnar, B. Popper, H. Liapis, A. M. Kotb, F. Siegerist, N. Endlich, H. J. Anders, MDM2 prevents spontaneous tubular epithelial cell death and acute kidney injury. *Cell Death Dis* **7**, e2482 (2016).
75. H. Kuwana, Y. Terada, T. Kobayashi, T. Okado, J. M. Penninger, J. Irie-Sasaki, T. Sasaki, S. Sasaki, The phosphoinositide-3 kinase gamma-Akt pathway mediates renal tubular injury in cisplatin nephrotoxicity. *Kidney Int* **73**, 430-445 (2008).
76. J. Zhou, Y. Fan, S. Tang, H. Wu, J. Zhong, Z. Huang, C. Yang, H. Chen, Inhibition of PTEN activity aggravates cisplatin-induced acute kidney injury. *Oncotarget* **8**, 103154-103166 (2017).
77. Q. Sun, Q. T. Meng, Y. Jiang, H. M. Liu, S. Q. Lei, W. T. Su, W. N. Duan, Y. Wu, Z. Y. Xia, Z. Y. Xia, Protective effect of ginsenoside Rb1 against intestinal ischemia-reperfusion induced acute renal injury in mice. *PLoS One* **8**, e80859 (2013).
78. T. Ito, J. D. Williams, D. Fraser, A. O. Phillips, Hyaluronan attenuates transforming growth factor-beta1-mediated signaling in renal proximal tubular epithelial cells. *Am J Pathol* **164**, 1979-1988 (2004).
79. G. Schley, B. Klanke, J. Schodel, F. Forstreuter, D. Shukla, A. Kurtz, K. Amann, M. S. Wiesener, S. Rosen, K. U. Eckardt, P. H. Maxwell, C. Willam, Hypoxia-inducible transcription factors stabilization in the thick ascending limb protects against ischemic acute kidney injury. *J Am Soc Nephrol* **22**, 2004-2015 (2011).

Acknowledgements: We thank L. Calosi, S. Catarinicchia and D. Guasti from the Department of Experimental and Clinical Medicine, University of Florence, Italy, for their technical support with sample preparation for histology. We thank B. Schäfer, University Children's Hospital, Zurich, Switzerland and A. Burger, University of Colorado Denver, USA, for the Pax2.rtTA mouse. **Funding:** This study was funded by the European Research Council under the Consolidator Grant RENOIR to P.R. (ERC-2014-CoG), grant number 648274, by the Associazione Italiana per la Ricerca sul Cancro (AIRC) and Fondazione CR Firenze under IG 2018 – ID.21821 project – to P.R.. A.J.P. is a recipient of the Fondazione Umberto Veronesi fellowship. H.J.A. was supported by the Deutsche Forschungsgemeinschaft AN372/24-1. **Author contributions:** P.R. designed the study. D.F., M.G., A. Minervini, S.S., M.C., A. Mari, F.D.M, A.A., F.P., R.S., V.F., C.F.C. and R.M.R collected patient clinical data, M.A., F.G., C.F.C and A. Mari analysed them. A.J.P., G.A., M.L.A., A.S. and L.D.C. performed immunohistochemistry and confocal microscopy. A.J.P., G.A., A.S., C.C., B.M., S.N. and M.E.M. designed and carried out experiments in the mouse system. G.J.N. and M.R.R. performed the histopathological tissue analysis of the mouse H&E samples. A.J.P., G.A., M.L.A., A.S. and P.R. analyzed the data. T.L. performed ultrasound imaging. S.L. and S.G. performed single cell RNA sequencing, R.S. and A. Magi. analysed the datasets. M.R., A.Mari, M.A. and F.G. performed statistical analysis. A.P., M.A., M.L.A., F.G., E.L., L.L., C.F.C., M.R., H.L., H.J.A. and M.R.R. critically reviewed the manuscript. P.R. and A.J.P. wrote the paper with input from all authors. **Competing interests:** H.L. receives NIH consultant fees for the CUREGN consortium**.** H.J.H does consulting for Astra-Zeneka, Janssen, GSK, Previpharma, Inositec, Secarna, NOXXON. All other authors declare that they have no competing interests. **Data and material availability:** Microarray and scRNAseq data are available in NCBI's Gene Expression Omnibus repository as GSE137704 and GSE137620, respectively. All data

associated with this study are present in the paper or the Supplementary Materials, or are available from The Human Protein Atlas (https://www.proteinatlas.org/).

Figures:

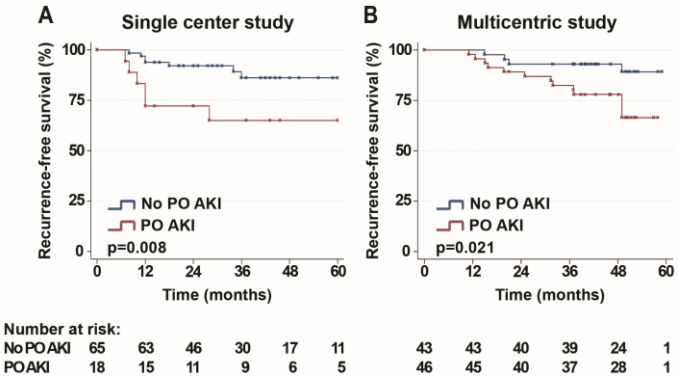

Fig. 1. Recurrence-free survival in patients with pRCC according to the presence or absence of a postoperative AKI episode. (**A, B**) pRCC patients' recurrence-free survival based on the presence or absence of a postoperative AKI episode in (**A**) a single center study (n=65 no postoperative AKI, n=18 postoperative AKI) and (**B**) a multicentric study (n=43 no postoperative AKI, n=46 postoperative AKI). Censored patients and patients at risk are shown. Kaplan-Meier curves are compared by log-rank test (7.143 and 5.36, respectively) and Cox regression ($HR_{(A)}$=3.6 [1.3-10.2]; $HR_{(B)}$=3.4 [1.1-10.3]). Statistical significance was set for a p-value <0.05. PO AKI: Postoperative AKI.

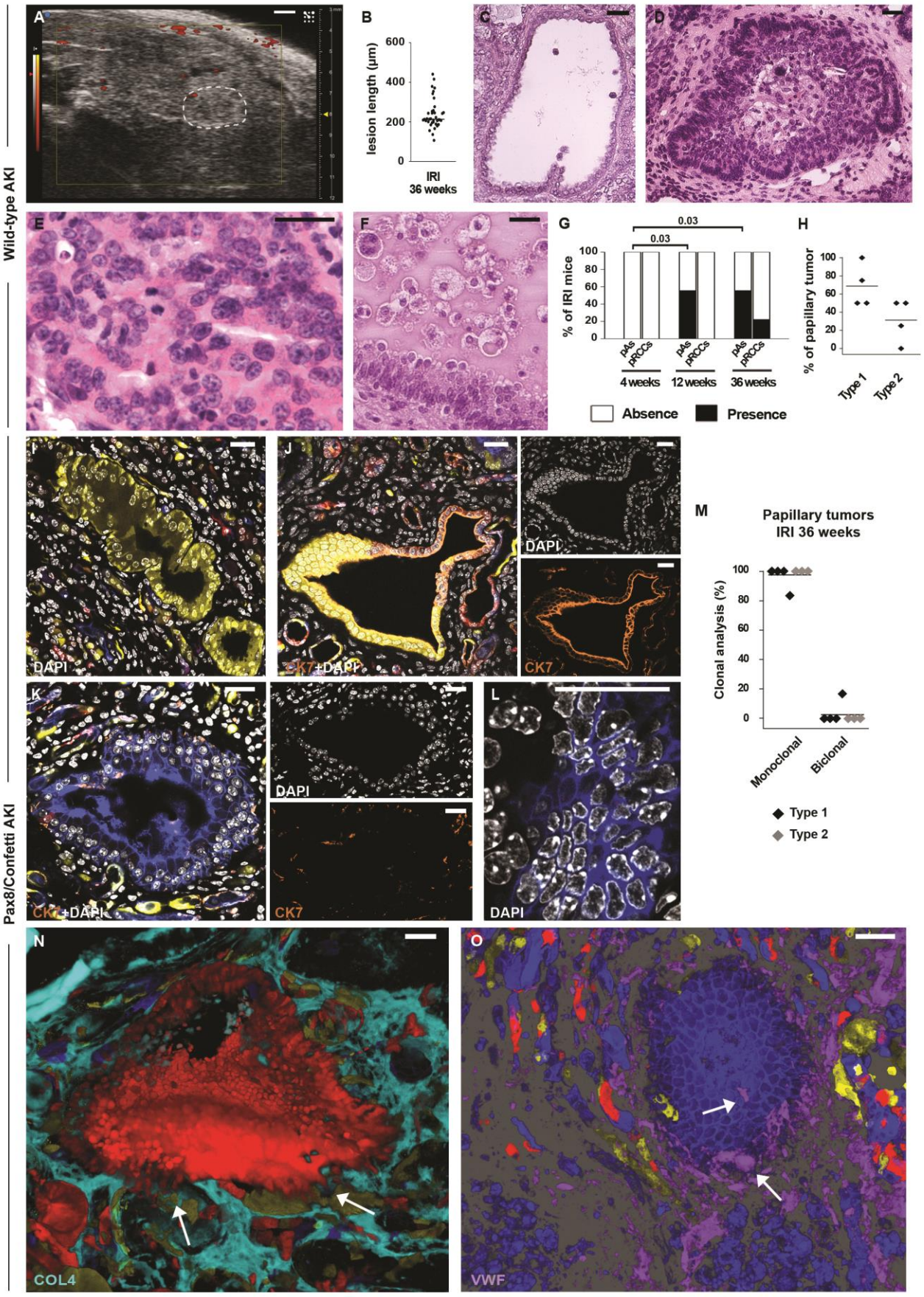
Wild-type AKI
Pax8/Confetti AKI
A
B
lesion length (µm)
600
400
200
0
IRI
36 weeks
C
D
E
F
G
0.03
0.03
% of IRI mice
100
80
60
40
20
0
pAs
pRCCs
4 weeks
12 weeks
36 weeks
Absence
Presence
H
% of papillary tumor
Type 1
Type 2
I
DAPI
J
CK7+DAPI
DAPI
CK7
K
CK7+DAPI
DAPI
CK7
L
DAPI
M
Papillary tumors
IRI 36 weeks
Clonal analysis (%)
Monoclonal
Biclonal
Type 1
Type 2
N
COL4
O
VWF

1

Fig. 2. Long-term follow-up reveals that AKI induces papillary tumors in mice. (**A)** Ultrasound image with Power Doppler Mode (red) of a wild-type mouse kidney (displayed in transverse plane) at 36 weeks after ischemia-reperfusion injury (IRI) (representative of n=3 mice). The region of interest (ROI, dashed line) indicates tumoral tissue. Bar=1 mm. (**B**) Length (µm) of the lesions in wild-type mouse kidneys at 36 weeks after IRI (n=5 mice). Bar indicates median value. (**C**-**F**) Representative histological images with H&E staining of papillary tumors from wild-type mouse kidneys after IRI. In (**C**), a type 1 papillary tumor. In (**D**), a type 2 papillary tumor. In (**E**), nuclear atypias. In (**F**), foamy macrophages within a papillary lesion. Bars=25 µm. (**G**) Percentages of mice at 4 weeks (n=8), 12 weeks (n=9), and 36 weeks (n=9) after IRI presenting with papillary adenomas (pAs) and pRCCs. Numbers above graph represent p-values. (**H**) Percentage of type 1 *vs.* type 2 papillary tumors in wild-type mice at 36 weeks after IRI (n=4 mice). Bars indicate mean values. No significant difference between the groups. (**I**) Representative confocal image of a type 1 papillary tumor from Pax8/Confetti mouse kidneys at 36 weeks after IRI. Bar=25 µm. (**J**) Split confocal images of CK7 staining (orange) of a type 1 papillary tumor from Pax8/Confetti mouse kidneys at 36 weeks after IRI. Bar=25 µm. (**K**) Split confocal images of CK7 staining (orange) of a type 2 papillary tumor from Pax8/Confetti mouse kidneys at 36 weeks after IRI. Bar=25 µm. (**L**) Detail of nuclear atypias in a type 2 papillary tumor from Pax8/Confetti mouse kidneys at 36 weeks after IRI. Bar=25 µm. (**M**) Clonal analysis in type 1 and 2 papillary tumors from Pax8/Confetti mouse kidneys at 36 weeks after IRI (n=7 mice). Bars indicates mean value. (**N, O**) 3D reconstruction of representative pRCC in Pax8/Confetti mouse kidneys at 36 weeks after IRI. In (**N**), collagen IV (COL4) staining (cyan). Arrows indicate invasion. In (**O**), Von Willebrand Factor (VWF) staining (purple). Arrows indicate tumor vascularization. Bars= 25 µm. DAPI (white) counterstains nuclei. Signals for fluorescent Confetti proteins are as follow: GFP, green; RFP, red; YFP, yellow, and CFP, blue. Statistical power was assessed using Fisher's exact test (**G**) or Mann-Whitney test (**H**). N.S ($p>0.05$).

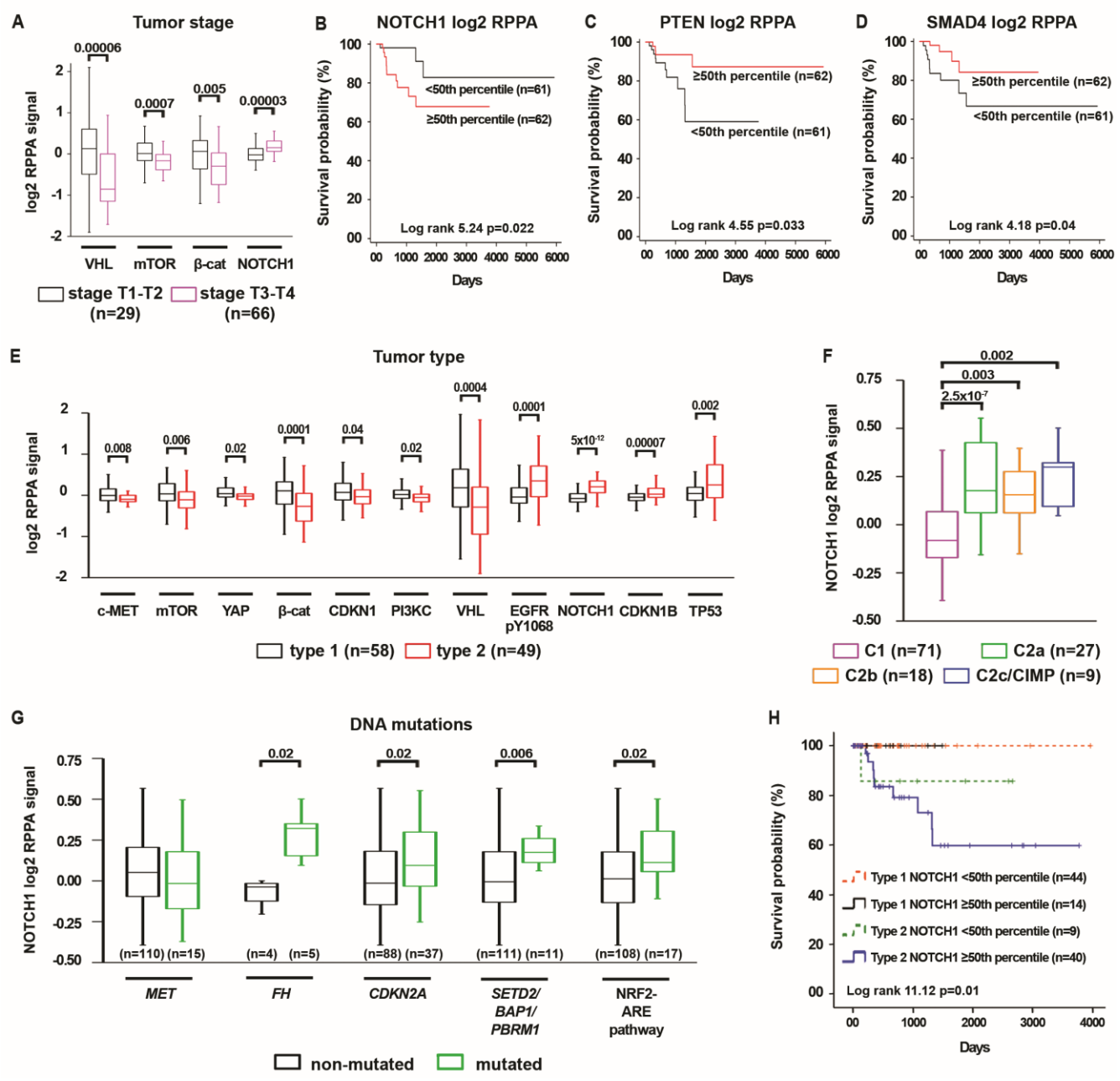

Fig. 3. NOTCH1 overexpression is specific for human type 2 pRCC and predicts poor prognosis. (**A**) Log2 RPPA signal for proteins differently expressed in tumor stage T1-T2 (black boxes, n=29 patients) vs T3-T4 (pink boxes, n=66) pRCC. (**B-D**) Overall survival of pRCC patients based on high (≥50th percentile, n=62) or low (<50th percentile, n=61) expression of different proteins: NOTCH1 (**B**), PTEN (**C**), or SMAD4 (**D**). (**E**) Log2 RPPA signal for proteins different in tumor type 1 (black box, n=58) vs. type 2 (red box, n=49) pRCC. (**F**) NOTCH1 log2 RPPA signal in patients with pRCC of

clusters C1, C2a, C2b, and C2c/CIMP (n=71, 27, 18, and 9, respectively). (**G**) NOTCH1 log2 RPPA signal in patients with non-mutated (black boxes) or mutated (green boxes) *MET* (non-mutated n=110, mutated n=15), *FH* (non-mutated n=4, mutated n=5), *CDKN2A* (non-mutated n=88, mutated n=37), *SETD2/BAP1/PBRM1* (non-mutated n=111, mutated n=11), or NRF2–antioxidant response element (ARE) pathway (non-mutated n=108, mutated n=17). (**H**) Differences in overall survival of patients with type 1 or type 2 pRCC based on high ($\geq 50^{th}$ percentile, type 1 n=14 and type 2 n=40) or low ($<50^{th}$ percentile, type 1 n=44 and type 2 n=9) NOTCH1 protein expression. β-cat: β-catenin. RPPA: reverse phase protein array. Box-and-whisker plots: line = median, box = 25-75%, whiskers = min-max. Statistical significance was calculated by Mann-Whitney test. Kaplan-Meier curves are compared by log-rank test and Cox regression ($HR_{(B)}$=4.0 [1.1-14.3]; $HR_{(C)}$=3.3 [1.0-10.8]; $HR_{(D)}$=3.2 [1.0-10.1]; $HR_{(F)}$=4.6 [1.0-20.5]). Numbers above graphs represent p-values.

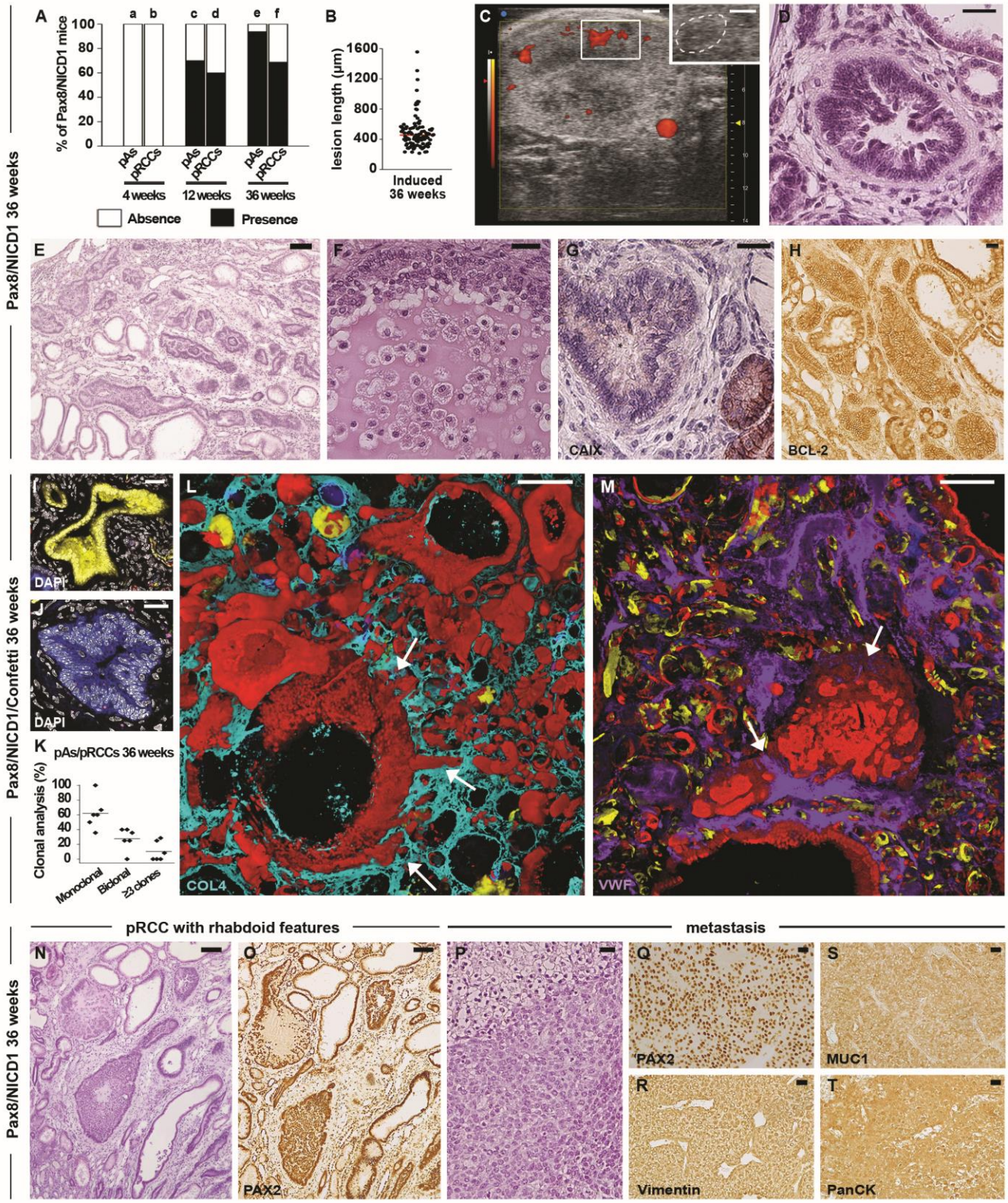

Fig. 4. NICD1 overexpression in mouse tubular cells induces clonal type 2 papillary tumors. (**A**) Percentages of Pax8/NICD1 mice at 4 weeks (n=8), 12 weeks (n=10), and 36 weeks (n=16) presenting

with papillary adenomas (pAs) and pRCCs. Statistical power was assessed using Fisher's exact test: a vs. c p=0.004, a vs. e p=0.0001, c vs. e p=0.2642 and b vs. d p=0.0128, b vs. f p=0.002, d vs. f p=0.6924. (**B**) Length (µm) of the lesions in Pax8/NICD1 mouse kidneys at 36 weeks (n=5 mice). Bar (red) indicates median value. (**C**) Ultrasound image with Power doppler Mode (red) of a wild-type mouse kidney (displayed in transverse plane) at 36 weeks (representative of n=4 mice). Inset: high magnification of the ultrasound appearance of a tumor area (dashed line). Bar=1 mm. (**D**) Representative image of H&E staining of papillary adenoma from Pax8/NICD1 mouse kidney at 36 weeks. Bar=25 µm. (**E**) Type 2 papillary carcinoma from Pax8/NICD1 mouse kidney at 36 weeks. Bar=100 µm. (**F**) H&E staining of foamy macrophages within a papillary lesion from Pax8/NICD1 mouse kidney at 36 weeks. Bar=25 µm. (**G**) Representative image of a carbonic anhydrase IX (CAIX) negative papillary tumor (brown) from Pax8/NICD1 mouse kidney at 36 weeks. Bar=25 µm. (**H**) BCL-2 positive papillary tumor (brown) from Pax8/NICD1 mouse kidney at 36 weeks. Bar=25 µm. (**I**) Representative type 2 papillary tumor from Pax8/NICD1/Confetti mouse kidney at 36 weeks. Bar=25 µm. (**J**) Representative type 2 papillary tumor from Pax8/NICD1/Confetti mouse kidney at 36 weeks. Bar=25 µm. (**K**) Clonal analysis of papillary tumors in Pax8/NICD1/Confetti mice at 36 weeks (n=6 mice). Bars indicate mean values. (**L, M**) 3D reconstruction of representative lesions in Pax8/NICD1/Confetti kidney. In (**L**), COL4 staining (cyan). Arrows indicate invasion. In (**M**), VWF staining (purple). Arrows indicate vascularization of the tumor. Bars=100 µm. (**N**, **O**) Low-power images of a papillary tumor with rhabdoid features. In (**N**), H&E staining. In (**O**), PAX2 staining (brown). Bars=100 µm. (**P-T**) Histologic images of a subcutaneous metastasis. In (**P**), H&E staining. In the upper part of the image, subcutaneous adipose tissue; in the lower part, metastatic tissue with rhabdoid features. In (**Q**), PAX2 staining (brown). In (**R**), vimentin staining (brown). In (**S**), MUC1 staining (brown). In (**T**), PanCK staining (brown). Bars=25 µm. DAPI (white) counterstains nuclei. Signals for fluorescent Confetti proteins are as follow: GFP, green; RFP, red; YFP, yellow; and CFP, blue.

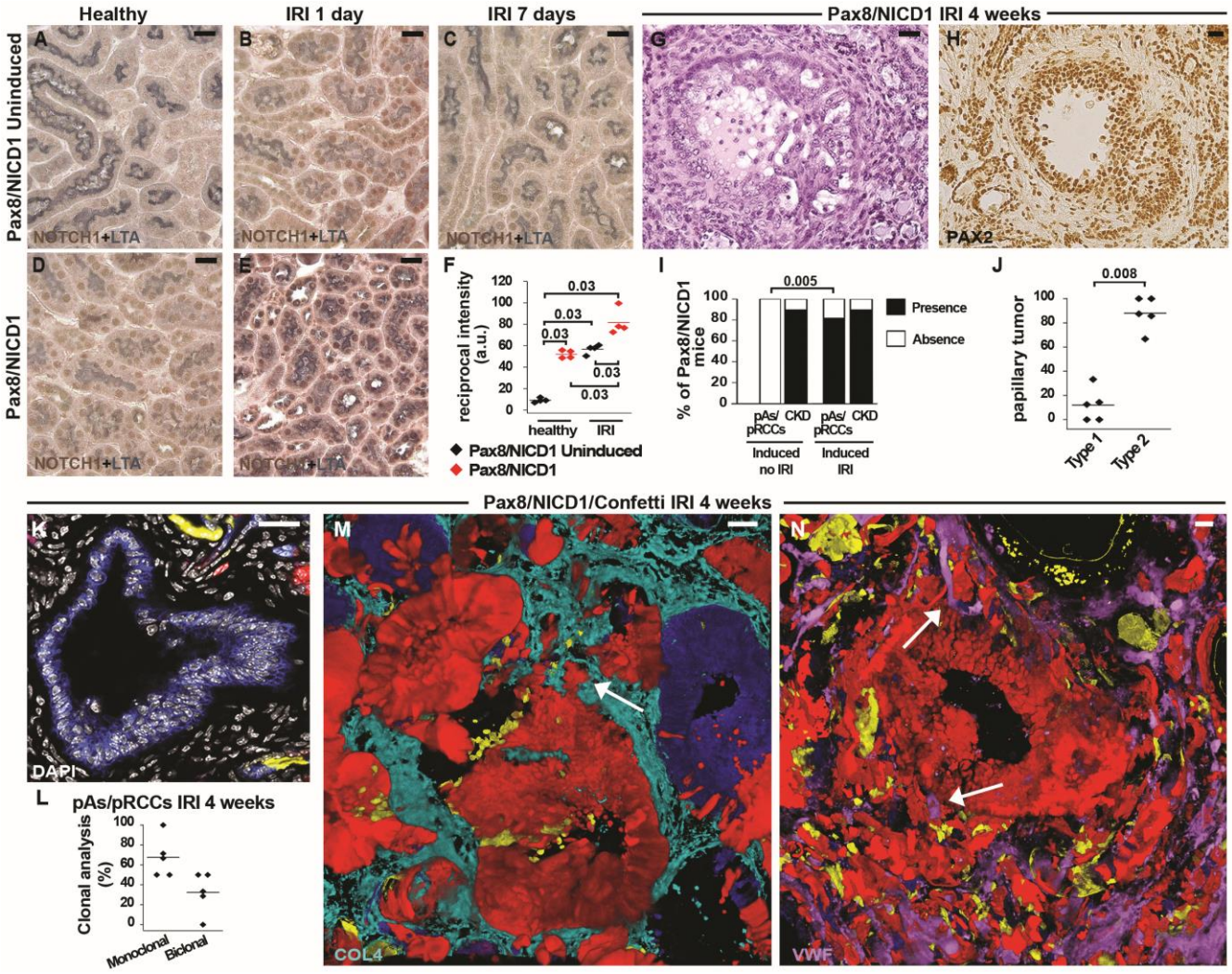

Fig. 5. AKI accelerates clonal type 2 papillary tumor development in mice. (**A**) Representative image of activated NOTCH1 staining (brown) and Lotus Tetraglonolobus Lectin (LTA, blue) in healthy uninduced Pax8/NICD1 mouse kidney at 1 day. Bar=25 µm. (**B**, **C**) Representative images of activated NOTCH1 staining (brown) and LTA (blue) in uninduced Pax8/NICD1 mouse kidney 1 day (**B**) and 7 days (**C**) after IRI. Bars=25 µm. (**D**) Representative image of activated NOTCH1 staining (brown) and LTA (blue) in healthy induced Pax8/NICD1 mouse kidney at 1 day. Bar=25 µm. (**E**) Representative image of activated NOTCH1 staining (brown) and LTA (blue) in induced Pax8/NICD1 mouse kidney 1 day after IRI. Bar=25 µm. (**F**) Graph of the reciprocal intensity of activated NOTCH1 per nucleus in uninduced and induced Pax8/NICD1 mice 1 day after IRI (n=4 mice for each group). a. u.: arbitrary units.

Bars indicate mean values. (**G**) Papillary tumor with foamy macrophages in the lumen, present in Pax8/NICD1 mice 4 weeks after IRI. Bar=25 µm. (**H**) PAX2 positive papillary tumor (brown) from Pax8/NICD1 mouse kidneys 4 weeks after IRI. Bar=25 µm. (**I**) Percentages of induced Pax8/NICD1 mice with or without IRI presenting with pAdenomas and pRCCs (pAs/pRCCs, n=5 uninduced and n=11 induced mice) and CKD (n=7 uninduced and n=5 induced mice) after 4 weeks. (**J**) Percentages of type 1 vs. type 2 papillary tumors in Pax8/NICD1 mice 4 weeks after IRI (n=5 mice). Bars indicate mean values. (**K**) Representative papillary tumor from Pax8/NICD1/Confetti mouse kidney 4 weeks after IRI. Bar=25 µm. DAPI (white) counterstains nuclei. (**L**) Clonal analysis of papillary tumors from Pax8/NICD1/Confetti mice 4 weeks after IRI (n=5 mice). Bars indicate mean values. (**M, N**) 3D reconstruction of representative lesions in Pax8/NICD1/Confetti kidneys after IRI. In (**M**), COL4 staining (cyan). Arrow indicates invasion. In (**N**), VWF staining (purple). Arrows indicate vascularization. DAPI (white) counterstains nuclei. Signals for fluorescent Confetti proteins are as follow: GFP, green; RFP, red; YFP, yellow; and CFP, blue. Bars 25 µm. Statistical power was assessed using Fisher's exact test (**I**) or Mann-Whitney test (**F, J**); numbers above graphs represent p-values.

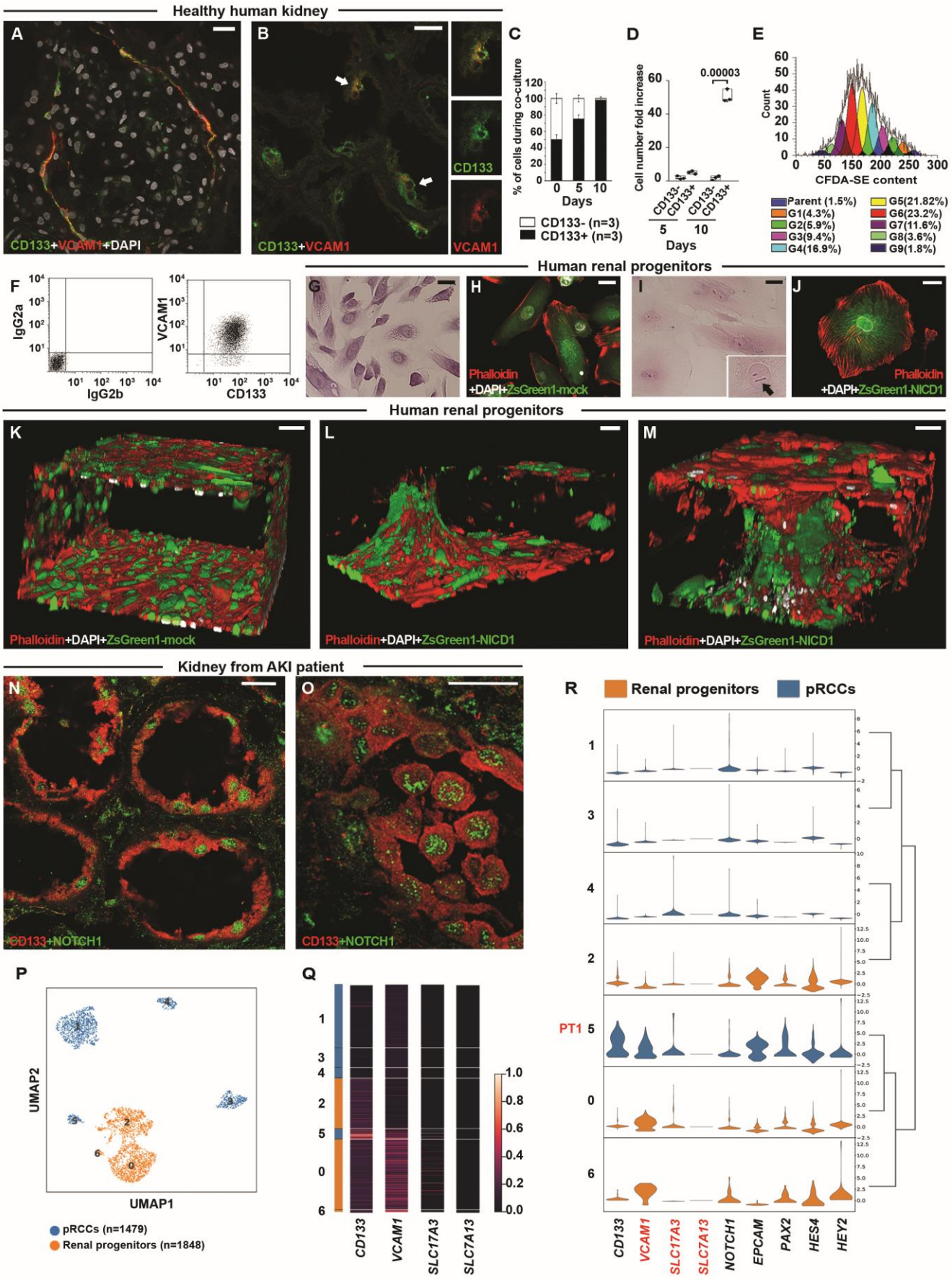
Healthy human kidney
A
CD133+VCAM1+DAPI
B
CD133+VCAM1
CD133
VCAM1
C
% of cells during co-culture
Days
CD133- (n=3)
CD133+ (n=3)
D
Cell number fold increase
0.00003
CD133- CD133+
CD133- CD133+
5
10
Days
E
Count
CFDA-SE content
Parent (1.5%)
G1(4.3%)
G2(5.9%)
G3(9.4%)
G4(16.9%)
G5(21.82%)
G6(23.2%)
G7(11.6%)
G8(3.6%)
G9(1.8%)
Human renal progenitors
F
IgG2a
IgG2b
VCAM1
CD133
G
H
Phalloidin
+DAPI+ZsGreen1-mock
I
J
Phalloidin
+DAPI+ZsGreen1-NICD1
Human renal progenitors
K
Phalloidin+DAPI+ZsGreen1-mock
L
Phalloidin+DAPI+ZsGreen1-NICD1
M
Phalloidin+DAPI+ZsGreen1-NICD1
Kidney from AKI patient
N
CD133+NOTCH1
O
CD133+NOTCH1
P
UMAP2
UMAP1
pRCCs (n=1479)
Renal progenitors (n=1848)
Q
CD133
VCAM1
SLC17A3
SLC7A13
R
Renal progenitors
pRCCs
PT1
CD133
VCAM1
SLC17A3
SLC7A13
NOTCH1
EPCAM
PAX2
HES4
HEY2

1

Fig. 6. Human renal progenitors are transformed by NOTCH1 overexpression. (**A**, **B**) Representative confocal images of healthy human kidney labelled with CD133 (green) and VCAM1 (red) (n=5 patients). In (**A**), glomerulus. In (**B**), tubules (arrows indicate CD133+VCAM1+ cells). Bars=25 µm. (**C**) Graph representing the evolution over time of the percentages of CD133+ and CD133- populations (n=3 biological replicates). (**D**) Graph representing the number of CD133- and CD133+ cells over time (n=3 biological replicates). Bars indicate median value. Statistical power was assessed using t test; number above graph represents p-value. (**E**) Representative cell division analysis of CFDA-SE-labeled CD133+ cells at day 10, out of 3 biological replicates. In the graph, the far right peak indicates undivided cells and each peak toward the left-hand side represents one cell division or generation. The percentages of cells in each division are shown in the graphs. (**F**) Representative FACS analysis for the contemporaneous expression of CD133 and VCAM1 in CD133+ fraction (right) and corresponding isotype controls (left) (n=3 biological replicates). (**G**, **H**) Representative H&E (**G**) and confocal (**H**) images of human renal progenitors infected with ZsGreen1-mock (n=3). In red, phalloidin staining. Bars=25 µm. (**I, J**) Representative H&E (**I**) and confocal (**J**) images of human renal progenitors infected with ZsGreen1-NICD1 (n=3) (black arrow indicates nuclear groove). In red, phalloidin staining. Bars=25 µm. (**K-M**) 3D reconstruction of a confocal z-stack of human renal progenitors infected with either ZsGreen1-mock (**K**) or ZsGreen1-NICD1 (**L, M**) and showing tubular morphology with a lumen (**K**) or growth towards inside the tubule lumen (**L**), generating a tumor-like mass (**M**) (1 representative image of n=3 biological replicates each). In red, phalloidin staining. Bars=50 µm. DAPI counterstains nuclei. (**N**) Representative confocal images of biopsies from patients with AKI (n=4). In red, CD133, in green activated NOTCH1. Bars= 25 µm. (**O**) Higher magnification of a representative confocal images of a biopsy from a patient with AKI (n=4). In red, CD133, in green activated NOTCH1. Bars= 25 µm. (**P**) UMAP representation of 3,327 cells, with 1479 pRCC (blue) and 1848 human renal progenitor (orange) cells. (**Q**) Expression of canonical PT1 signature and renal progenitor (*PROM1*) genes. (**R**) Violin plots

of single cell RNA sequencing data from pRCC (blue) (*32*) and from human renal progenitor cell cultures (orange), showing the expression of selected marker genes. In red, genes of the PT1 signature. *VCAM1*: vascular cell adhesion molecule 1, *EPCAM*: epithelial cell adhesion molecule, *SLC17A3*: Solute carrier family 17 member 3 and *SLC7A13*: Solute carrier family 7 member 13, CFDA-SE: Carboxyfluorescein diacetate succinimidyl ester.

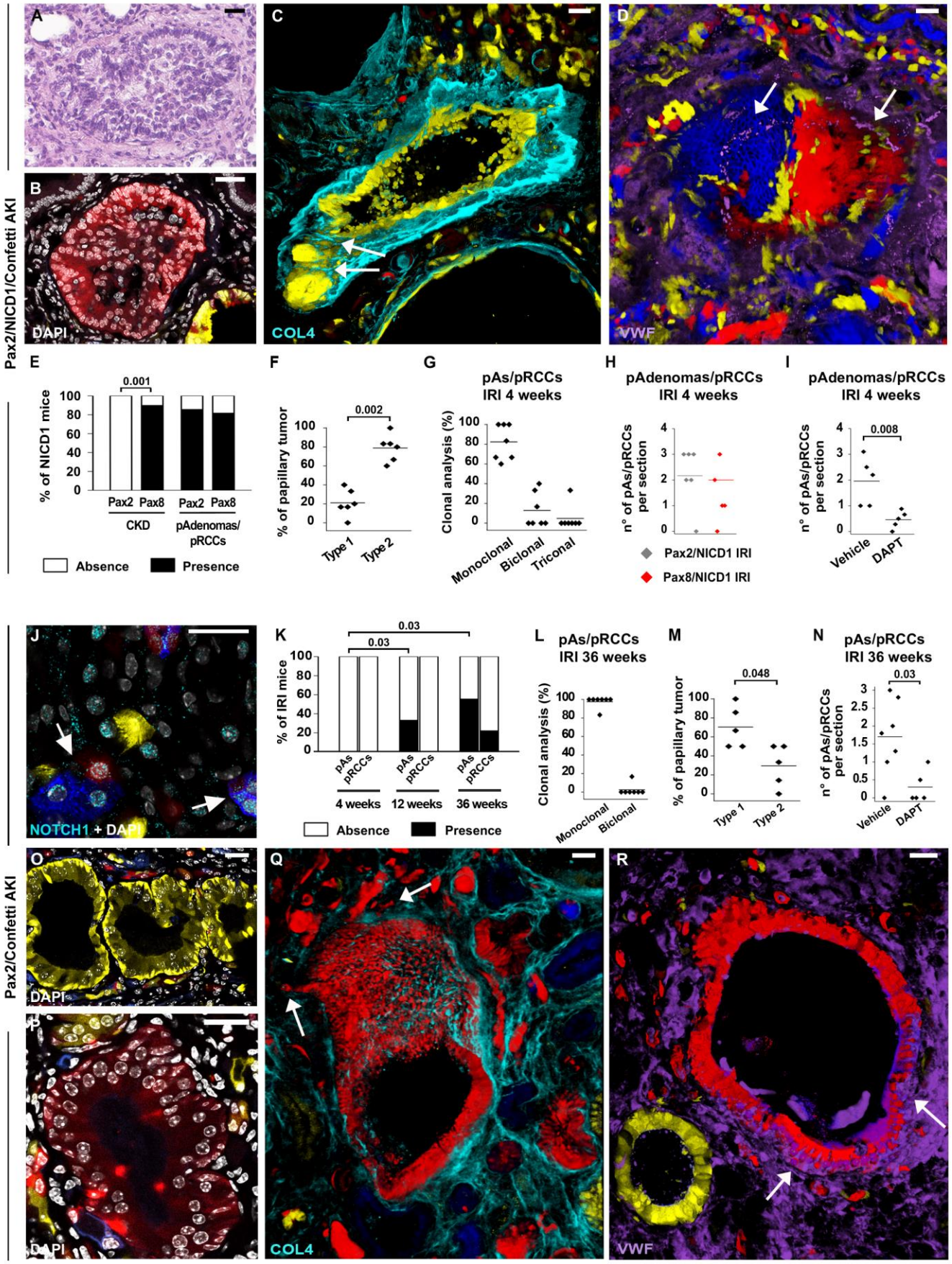
Pax2/NICD1/Confetti AKI
A
B
DAPI
C
COL4
D
VWF
E
0.001
% of NICD1 mice
Pax2 Pax8 Pax2 Pax8
CKD
pAdenomas/ pRCCs
Absence
Presence
F
0.002
% of papillary tumor
Type 1
Type 2
G
pAs/pRCCs IRI 4 weeks
Clonal analysis (%)
Monoclonal
Biclonal
Triconal
H
pAdenomas/pRCCs IRI 4 weeks
n° of pAs/pRCCs per section
Pax2/NICD1 IRI
Pax8/NICD1 IRI
I
pAdenomas/pRCCs IRI 4 weeks
0.008
n° of pAs/pRCCs per section
Vehicle
DAPT
J
NOTCH1 + DAPI
K
0.03
0.03
% of IRI mice
pAs pRCCs
4 weeks
12 weeks
36 weeks
Absence
Presence
L
pAs/pRCCs IRI 36 weeks
Clonal analysis (%)
Monoclonal
Biclonal
M
0.048
% of papillary tumor
Type 1
Type 2
N
pAs/pRCCs IRI 36 weeks
0.03
n° of pAs/pRCCs per section
Vehicle
DAPT
Pax2/Confetti AKI
O
DAPI
P
DAPI
Q
COL4
R
VWF

1

Fig. 7. AKI induces papillary tumors by promoting clonal expansion of renal progenitors in mice. (**A**) Representative histological image with H&E staining of a type 2 papillary carcinoma present in Pax2/NICD1 mice 4 weeks after IRI. Bar=25 µm. (**B**) Representative confocal image of type 2 papillary tumor of Pax2/NICD1/Confetti mice 4 weeks after IRI. Bar=25 µm. (**C**, **D**) 3D reconstruction of representative lesions in Pax2/NICD1/Confetti kidneys 4 weeks after IRI. In (**C**), COL4 staining (cyan). Arrows indicate invasion. In (**D**), VWF staining (purple). Arrows indicate vascularization of the tumor. Bars=25 µm. (**E**) Percentages of Pax2/NICD1 and Pax8/NICD1 mice presenting with pAdenomas and pRCCs (pAs/pRCCs) (n=11 for Pax2/NICD1 and n=11 for Pax8/NICD1) and CKD (n=6 for Pax2/NICD1 and n=5 for Pax8/NICD1) 4 weeks after IRI. (**F**) Percentages of type 1 vs. type 2 papillary tumors in Pax2/NICD1 mice 4 weeks after IRI (n=6 mice). Bars indicate mean values. (**G**) Clonal analysis of papillary tumors in each Pax2/NICD1/Confetti mouse 4 weeks after IRI (n=7 mice). Bars indicate mean value. (**H**) Graph of the number of papillary tumors per kidney section in Pax2/NICD1 (n=6) and Pax8/NICD1 (n=6) mice 4 weeks after IRI. Bars indicate mean values. No significant difference between the groups. (**I**) Graph of the number of papillary tumors per kidney section in Pax2/NICD1/Confetti mice treated with vehicle (n=5 mice) or DAPT (n=5 mice) and sacrificed 4 weeks after IRI. Bars indicate mean values. (**J**) Representative confocal image of activated NOTCH1 (cyan) in Pax2/Confetti mice 2 days after IRI (n=4). Arrows indicate Pax2+Notch1+ cells. Bar=25 µm. (**K**) Percentages of Pax2/Confetti mice at 4 weeks (n=8), 12 weeks (n=3), and 36 weeks (n=9) after IRI presenting with papillary adenomas (pAs) and pRCCs. (**L**) Clone frequency analysis in papillary tumors of Pax2/Confetti mouse kidneys at 36 weeks (n=7 mice). Bars indicate mean values. (**M**) Percentages of type 1 vs. type 2 papillary tumors in Pax2/Confetti mice at 36 weeks (n=5 mice). Bars indicate mean values. (**N**) Graph of the numbers of papillary tumors per kidney section in Pax2/Confetti mice treated with vehicle (n=7) or DAPT (n=5) and sacrificed 36 weeks after IRI. Bars indicate mean values. (**O, P**) Representative confocal images of type 1 (**O**) and type 2 (**P**) papillary tumors of Pax2/Confetti mice 36

weeks after IRI. Bars=25 µm. (**Q, R**) 3D reconstruction of representative lesions in Pax2/Confetti kidney 4 weeks after IRI. In (**Q**), COL4 staining (cyan). Arrows indicate invasion. In (**R**), VWF staining (purple). Arrows indicate vascularization of the tumor. Bars=25 µm. DAPI (white) counterstains nuclei. Signals for fluorescent Confetti proteins are as follow: GFP, green; RFP, red; YFP, yellow; and CFP, blue. Data are mean±SEM. Statistical power was assessed using Fisher's exact test (**E, K**) or Mann-Whitney test (**F, H, I, M, N**); numbers above graphs represent p-values.

	pRCC (n=56)	Controls (n=101)	*P* [(a)]
Previous AKI episodes	**12/56 (21.4%)**	**7/101 (6.9%)**	**0.008**
Age at surgery (years)	65.3 ± 11.7	63.7 ± 9.9	0.184
Gender (male)	**47/56 (83.9%)**	**65/101 (64.4%)**	**0.009**
Preoperative CKD (eGFR < 60)	10/56 (17.9%)	11/101 (10.9%)	0.219
DM	8/56 (14.3%)	14/101 (13.9%)	0.942
Length of follow-up (years)	4.6 ± 2.8	4.3 ± 2.9	0.571
Variable	**OR**	**(95%CI)**	***P*** [(b)]
AKI (y/n)	**3.479**	**(1.135 - 10.667)**	**0.029**
Age (years)	0.979	(0.947 - 1.012)	0.213
Gender (M/F)	2.907	(1.250 - 6.761)	0.013
CKD (y/n)	1.093	(0.377 - 3.163)	0.870
DM (y/n)	0.715	(0.258 - 1.978)	0.518
	ccRCC (n=75)	**Controls (n=101)**	***P*** [(a)]
Previous AKI episodes	9/75 (12.0%)	7/101 (6.9%)	0.247
Age at surgery (years)	**66.6 ± 9.3**	**63.7 ± 9.9**	**0.047**
Gender (male)	48/75 (64.0%)	65/101 (64.4%)	0.961
Preoperative CKD (eGFR < 60)	12/75 (16.0%)	11/101 (10.9%)	0.320
DM	11/75 (14.7%)	14/101 (13.9%)	0.880
Length of follow-up (years)	4.2 ± 2.2	4.3 ± 2.9	0.916
Variable	**OR**	**(95%CI)**	***P*** [(b)]
AKI (y/n)	1.549	(0.514 - 4.664)	0.437
Age (years)	0.971	(0.939 - 1.004)	0.085
Gender (M/F)	0.945	(0.516 - 1.852)	0.945
CKD (y/n)	1.202	(0.463 – 3.115)	0.706
DM (y/n)	0.888	(0.366 - 2.155)	0.793

Table 1. AKI episodes are a risk factor for the development of pRCC but not for ccRCC in humans. Clinical characteristics of pRCC, ccRCC and controls are described. Between-group comparisons were performed using the Mann–Whitney U test for continuous variables or the chi-squared test for categorical variables. Binary logistic regression analysis was used for the association between previous acute kidney injury (AKI) episodes (yes/no) and pRCC development adjusted for age, gender, preoperative chronic kidney disease (CKD), and diabetes mellitus (DM). eGFR, estimated glomerular filtration rate; OR, odds

ratio; RCC, renal cell carcinoma; pRCC: papillary RCC; ccRCC: clear cell RCC; SD, standard deviation; CI, confidence interval. Continuous variables are presented as mean±SD.